Advances in Applied Mathematics and Mechanics
Adv. Appl. Math. Mech., Vol. **x**, No. 1, pp. 1-42

DOI: 10.4208/aamm.OA-2023-0124
xxx 202x

Nonlinear Vibroacoustic Analysis of Functionally Graded Plates in the Thermal Ambiance at Oblique Incidence

F. Samadani and S. Roohollah Kazemi*

Faculty of Mechanical Engineering, University of Guilan, Rasht, Iran

Received xxx 2023; Accepted (in revised version) xxx 2024

Abstract. In this investigation, the analysis of the nonlinear vibroacoustic and sound transmission loss behaviors of plates made of functionally graded material is presented. It is assumed that the properties of the functionally graded plates are in the form of the simple power law scheme and continuous along the thickness, under thermal load and incident oblique plane sound wave as well as the first-order shear deformation theory. For this purpose, first, using Hamilton's principle, the nonlinear partial differential equations of motion are derived by the displacement field function approach and by considering the nonlinear von Kármán strain-displacement relations. To solve the equations, using the Galerkin method, the nonlinear partial differential equations of motion lead to Duffing equation. Then, using the homotopy analysis method, the equation of the transverse movement of the plate is solved semi-analytically to obtain the nonlinear frequencies. Finally, the nonlinear vibration and acoustic response of functionally graded plates are studied by considering the variation of the important parameters such as aspect ratio, dimensionless amplitude, volume fraction power of functionally graded material, external acoustic pressure, incidence and azimuthal angles, temperature changes, phase portrait, sound transmission loss, velocity and average mean square velocity of drive point and sound power level of the functionally graded plate. Results show increasing the incidence angle leads increase in hardening effects and sound transmission loss, but growing the azimuthal angle does not have much effect on the frequency-response and sound transmission loss in the absence of the external mean flow. Also, increasing temperature changes lead to decrease in hardening effects and sound transmission loss.

AMS subject classifications: to be provided by authors

Key words: Nonlinear vibroacoustic, functionally graded plate, first-order shear deformation theory, displacement field function approach, homotopy analysis method.

---

*Corresponding author.
Email: kazemi@guilan.ac.ir (S. Kazemi)

1 Introduction

Noise transmission is a crucial subject in the design of many structures, such as walls and floors of buildings, ship hulls, and side walls, and airplane and train cabins; Because noise, in addition to harassing the crew and passengers, may lead to fatigue of the structure and even catastrophic failures in the system. As a result, over the years, various analytical models have been presented and developed to predict the characteristics of the sound transmission. These models may be further classified as high-frequency or low-frequency noise models. In high-frequency noise, the panel dimensions are vast compared to relatively short sound wavelengths; therefore, the panel can be modeled analytically using the infinite panel theory. In low-frequency noise, panel dimensions are comparable to long-wavelength sound, and boundary effects are essential. In this approach, the panel is usually modeled as a rectangular simply supported plate in an infinite baffle. When a panel with infinite length is acoustically excited, the frequency at which the speed of sound in the air equals the speed of the free bending wave is named the critical frequency [1]. Critical frequency is especially significant when dealing with sound radiation from structures. The characteristics of sound radiation depend on whether the incitement frequency is higher or lower than the critical frequency. Similarly, the sound radiation efficiency of structure is very high near the critical frequency. The behavior of plates with limited length is shown in the same way. When a structure is acoustically excited, the frequency at which the speed of the free bending wave equals the speed of the forced bending wave is called the coincidence frequency [1]. Sound transmission close to the coincidence frequency is very high. Sound transmission characteristics hinge on whether the incitement frequency is higher or lower than the coincidence frequency. The vibrational response of a plate to the sound field around its critical frequency is the greatest. So, to find the structure response to sound incitement, it is necessary to know its critical frequency precisely. If it is necessary to reduce the response, the critical frequency information of the structure can be applied in its plan. For instance, the structure can be planned so that the critical frequency is outside the kind of frequencies in which the acoustic incitement is greater. Therefore, knowing the information about the critical and coincidence frequencies of structure is necessary to learning its structural-acoustic relations. It should be intentioned that these two parameters are interdependent. The critical and coincidence frequencies of the plates have been debated in particular in references [2–4].

Functionally graded materials (FGM) are composite materials whose mechanical or thermal specifications vary functionally and continuously from one level to another. The use of FGM in recent decades is a significant increase. Since these materials have high thermal resistance, they have many engineering usages in productions, for example, defense and aerospace productions. Also, these materials are applied in the structure of tools, for example, nuclear reactors, turbine blades, pressure vessels, heat exchangers, biomedical materials such as dental implants, and chemical productions. Panels are one of the common structures made of FGM that have many uses in engineering constructions, for example, space vehicles, and different parts of the airplane, and are used mainly in civil buildings. So, because these materials are significant, much research has been done on the vibration of functionally graded (FG) plates. Considering that in the classical plate theory (CPT), shear deformations in the thickness of the panel are ignored, the natural frequencies are obtained with a little approximation. To solve this problem, it is possible to study the vibration of panels by applying the first-order shear deformation theory (FSDT) or higher-order shear deformation theory (HSDT). Considering that for the accurate and reliable design and analysis of a structure, it is necessary to investigate the vibration with large amplitude, in reality, most phenomena are nonlinear, and as a result, nonlinear analysis is closer to reality than linear analysis. For this purpose, in this paper, von Kármán's nonlinear strain-displacement relationships are used to study the nonlinear vibration of the FG plate.

Damping is an essential factor in the dynamic design of many engineering components because it significantly affects the level of vibration and noise. It also controls the fatigue life and impact resistance of structures [5]. FGMs have higher inherent damping than conventional isotropic materials due to the interaction between metal and ceramic. FGMs are widely used in the automotive, marine, and aerospace industries due to their high hardness-to-weight ratio and play a significant role in reducing input noise to mechanical systems. These materials are widely used due to their simplicity and inexpensive. For example, to control the noise entering the airplane cabin, FGMs are commonly used in the middle compartment of the panels. Therefore, there is a critical necessity to gain an appearance for the critical, coincidence frequencies, and sound transmission loss (STL) of the plates, taking into account the orthotropic behavior and crosswise shear flexibility and investigating the effects of the incidence angle in addition to the azimuthal angle.

Considering the importance and application of FGM, some researchers conducted studies on the mechanical behavior of these materials. Gholami and Ansari [6] studied the forced vibrations of FG plates based on the theory of three-dimensional elasticity theory in different boundary conditions. Hashemi and Jafari [7] analyzed the nonlinear free vibration of a rectangular plate made of FGM using the FSDT. Thai et al. [8] investigated the free vibration and bending of a rectangular plate made of FGM using the simplified FSDT. Singh and Harsha [9], studied the static analysis of the functionally graded rectangular plate using von Kármán's nonlinear classical plate theory. Several researchers investigated the vibration of plates made of FGM based on CPT. Yazdi [10] analyzed the nonlinear free vibration of a thin plate made of FGM using the homotopy perturbation method (HPM) and based on CPT. Some researchers studied the linear vibrations of FG plates using the FSDT or HSDT. Yang and Shen [11] analyzed the free and forced vibration of sheets made of [12] analyzed the stability, and free vibrations of plates made FGM by using two-dimensional HSDT. Vel and Batra [13] investigated the free and forced linear vibrations of rectangular plates made of FGM based on the three-dimensional elastic theory with simply supported boundary conditions by using the power series solution and by comparing the results obtained from the CPT, FSDT and third-order shear deformation theory (TSDT) showed that for functionally graded materials, a more accurate solution is obtained from the FSDT than the TSDT. For this purpose, in this paper, the FSDT is used to study the nonlinear vibration of an FG plate. Some other researchers investigated the nonlinear vibration of FGMs. Hao et al. [14] analyzed the nonlinear dynamics of a single-walled rectangular plate made of FGM in a thermal ambiance under external transverse loading. They used HSDT and finally found the nonlinear dynamic resonances of the plate by using an approximate perturbation method and the Runge-Kutta numerical method. Zhang et al. [15] analyzed the nonlinear dynamics of a circular joint plate made of FGM under external and parametric loads created on the HSDT and using an approximate perturbation method based on Fourier expansion. Dogan [16] investigated the nonlinear vibrations of a cantilever plate made of FGM under random excitation. Huang and Shen [17, 18] investigated the nonlinear vibration and dynamic response of FG plates and shells in thermal environments by using the HSDT and perturbation methods. Samadani et al. [19] investigated the nonlinear vibrations of two models of nanobeams using the homotopy analysis method (HAM) [20].Torabi et al. [21] analyzed the dynamic instability of nanoplates made of FGM using the HAM in different boundary conditions. Yoosefian et al. [22] studied the nonlinear bending of sandwich plates made of FGM under mechanical and thermal loads.

The issue of sound behavior and sound transmission in panels has been investigated by various researchers. Amirinejad et al. [23] conducted sound wave transmission from a polymer foam plate using the mathematical model of the functionally graded viscoelastic materials (FGV). Li et al. [24] studied the effects of distributed mass loading on the sound radiation behavior of plates. Huang et al. [25] investigated the sound transmission of sandwich panels using three-dimensional elasticity theory. Xin et al. [26] analyzed the sound transmission of a two-part metal panel under acoustic excitation by an analytical method. Zhang et al. [27] discussed a unified approach to predict acoustic radiation from rectangular plates with arbitrary boundary conditions. Hu et al. [28] analyzed the sound radiation from functionally graded porous plates (FGP) with arbitrary and stationary boundary conditions on an elastic foundation. Arasan et al. [29], using wave number analysis, obtained analytical expressions for the frequency limit of thin and thick plates for an elastic layer of isotropic materials and were able to predict its vibroacoustic behavior. Zhou et al. [30], investigated the vibrations and sound radiation of FG plates under the temperature gradient along the thickness of the plate. Yang and Shen [11] analyzed the vibroacoustic response of the FG plate exposed to the thermal ambiance with the CPT and the FSDT semi-analytically (differential quadrature approximation, Galerkin technique, and the modal superposition method). Chandra et al. [31], analyzed the loss of sound transmission and vibroacoustic of an FG plate with the FSDT. Geng et al. [32] studied the vibration and sound radiation characteristics of a thin isotropic plate in thermal ambiance. Oliazadeh et al. [33] studied sound transmission from single-layer and double-layer rectangular plates using statistical energy analysis (SEA) [34] to predict the sound transmission loss of the single and double-walled plates. Yang et al. [35] studied the sound radiation from an FG plate using the theory of three-dimensional elasticity and considering the state space method [36].

Various solution methods have been applied to investigate the vibroacoustic of structures. Some numerical methods such as the finite element method (FEM), the boundary element method (BEM), the Durbin's numerical Laplace transform inversion scheme, the Rayleigh integral method [37], multiple time-scales method (MTSM) [38], reduced-order method [39], have been presented in literature. Dhainaut et al. [40] presented a finite element formulation to predict the nonlinear random response of thin isotropic composite panels simultaneously exposed to high sound loads and temperatures. Jeyaraj et al. [5], studied the vibration-sound response of a plate made of composite materials in a thermal ambiance with the technique of combining BEM with FEM and considering the inherent damping of the plate and loss factor. Norouzi and Younesian [41], using Durbin's numerical Laplace transform inversion scheme, the Rayleigh integral method, and the MTSM investigated the vibroacoustic issue for a viscoelastic rectangular plate with a nonlinear geometry exposed to a subsonic compressible airflow. In [35], the Rayleigh integral method has been employed to calculate the sound radiation of the vibration plate. Przekop and Rizzi [42] analyzed the dynamic response of a combined sound-heat load of a thin aluminum beam subjected to a sudden and intense impact with the reduced-order method. Some analytic approximation methods such as the Adomian decomposition method (ADM) [43] and HAM have been considered in the literature. In [41], the ADM has been applied to solve the nonlinear vibroacoustic equation of a viscoelastic rectangular plate and in [44], HAM is applied to obtain the solution of surface acoustic waves in an FG plate. Some analytical methods such as the convergent power series solution [45] and the transfer matrix method [46] have been applied in the literature. In [47], the convergent power series solution is applied to obtain the exact dynamic response of the truncated conical shell and in [25], the transfer matrix method is used to develop the analytical solutions of sound transmission through sandwich panels.

However, the issue of nonlinear vibroacoustic of panels has been investigated by a few researchers. Kim et al. [48] investigated the nonlinear random response of thin and thick panels under combined sound-heat load using FSDT and von Kármán's nonlinear classical plate theory. Therefore, the need for nonlinear vibroacoustic analysis of panels made of FGM is more noticeable than before. In this paper, due to the presence of nonlinear parameters and to accurately check the effect of these parameters and also provide an approximate expression for the nonlinear frequency (ω_{NL}) of the system, a semi-analytical method is used to solve the governing nonlinear equation. For this purpose, the HAM is used to solve the nonlinear differential equations governing the vibroacoustic of a plate made of FGM with a simply supported boundary condition. In this approach, by applying the Galerkin method, the nonlinear partial differential equations of motion are reduced into nonlinear ordinary differential equations in the time domain. The resulting equations are dimensionless and they are solved using the HAM to analyze the effects of different parameters on sound transmission loss and vibration response of the system with an approximate analytical solution.

In this investigation, the homotopy analysis method and the Galerkin method [49,50] are applied to study the nonlinear vibroacoustic analysis of functionally graded plates in the thermal ambiance at oblique incidence. The outline of this paper is as follows: In Section 2, by using von Kármán's nonlinear strain-displacement relations and the first-order shear deformation theory, taking into account the specifications of the functionally graded plate and the sound pressure characteristics, the equations of motion are derived using Hamilton's principle. Then, the governing nonlinear partial differential equations of the functionally graded plate are converted to nonlinear ordinary differential ones in the time domain through applying the Galerkin method. Then, the obtained equations are reduced to one equation which is solved in Section 3 using the homotopy analysis method. In Section 4, to calculate the free field sound radiation associated with a given vibration response, an acoustic model of functionally graded plate is considered. Then, in Section 5, the effects of different parameters such as aspect ratio, dimensionless amplitude, volume fraction power of functionally graded material, external acoustic pressure, incidence and azimuthal angles, temperature changes, phase portrait, sound transmission loss, velocity and average mean square velocity of drive point and sound power level on the nonlinear vibration and acoustic responses of the functionally graded plates are investigated. Finally, in Section 6, conclusions are provided.

2 Mathematical modeling and governing equations

The main feature of FGM is a mixture of ceramic and metal. Its properties, including Young's modulus, thermal expansion coefficient, Poisson's ratio, mass density, and thermal conductivity, constantly change along the thickness of the plate, and the power law is used to present the volume fraction of ceramic and metal phases. There are different models for the homogenization of FGM components. If the changes in material properties along the thickness are slow, it is possible to use the standard plan in the scale of the representative volume element (RVE), but if the changes in the material properties along the thickness are fast, more advanced averaging methods such as Mori-Tanaka [51] and self-consistent methods should be used. Therefore, a wide variety of grading, from slow change to fast change of characters, is possible for metal-ceramics [52].

2.1 Specifications of FG plate

Fig. 1 shows the image of a plate made of FGM with length, l_a width l_b and thickness h, whose upper surface $(z=\frac{h}{2})$ is made of ceramic (indicated by the subscript c in the formulas), and its lower surface $(z=-\frac{h}{2})$ is made of metal (indicated by the subscript m in the formulas); under oblique sound pressure it shows two angles of incident and azimuthal. Since structures made of FGMs are most commonly used in high temperature ambiance where significant changes in mechanical properties of the constituent materials are expected, it is essential to take into consideration this temperature-dependency for accurate prediction of the mechanical response.

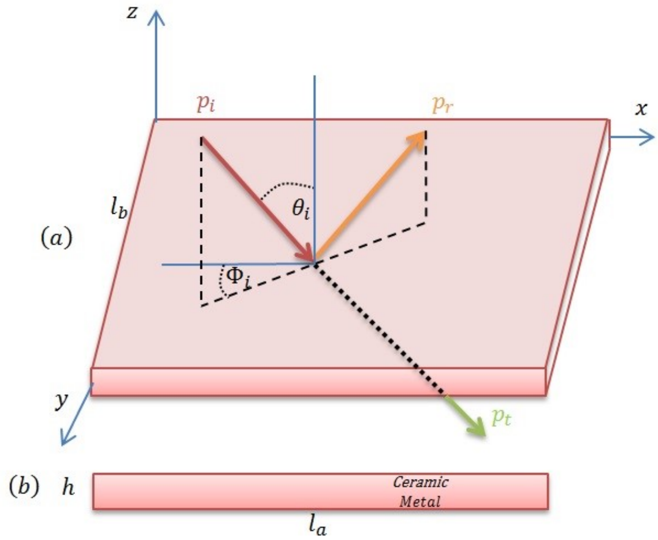

Figure 1: Schematic of an FG plate under oblique acoustic load.

In FGM structures, the generic material properties are assumed to be functions of temperature and thickness direction z [18]:

$$P(z,T)=P_t(T)V_c(z)+P_b(T)V_m(z),$$

where $P(z,T)$ represents the effective properties of this plate such as Young's modulus E, thermal expansion coefficient α, Poisson's ratio ϑ, mass density ρ, and thermal conductivity κ.$P_t(T)$ and $P_b(T)$ are the properties at the top and bottom surfaces of the FG plate that are assumed to be temperature-dependent, whereas the mass density is independent to the temperature. $V_c(z)$ and $V_m(z)=1-V_c(z)$ are the ceramic and metal volume fractions. $V_c(z)$ follows a simple power law as:

$$V_c(z)=\left(\frac{1}{2}+\frac{z}{h}\right)^n,$$

where n is the index of the power law and dictates whether the FGM is rich in ceramic or metal. According to the power law, $n=0$ indicates an entirely ceramic state, and $n=\infty$ defines an entirely metallic state. The properties of the top and bottom surfaces of the FG plate can be formulated as a nonlinear function of temperature as follows [18]:

$$P=P_0(P_{-1}T^{-1}+1+P_1T+P_2T^2+P_3T^3),$$

in which the constants P_0, P_{-1}, P_1, P_2 and P_3 are the coefficients of the temperature $T(K)$ and are specific for each material, T is the temperature at an arbitrary material point of the plate. According to a simple rule of mixture of composite materials (Voigt model), the effective properties of an FG plate can be written as [18]:

$$\begin{aligned}
&E(z,T)=[E_c(T)-E_m(T)]V_c(Z)+E_m(T),\\
&\alpha(z,T)=[\alpha_c(T)-\alpha_m(T)]V_c(Z)+\alpha_m(T),\\
&\kappa(z,T)=[\kappa_c(T)-\kappa_m(T)]V_c(Z)+\kappa_m(T),\\
&\vartheta(z,T)=[\vartheta_c(T)-\vartheta_m(T)]V_c(Z)+\vartheta_m(T),\\
&\rho(z,T)=(\rho_c-\rho_m)V_c(Z)+\rho_m.
\end{aligned}$$

Three cases of temperature change across the thickness of the plate are considered, i.e., uniform temperature rise, nonlinear temperature rise and linear temperature rise. In uniform case, temperature field is expressed as:

$$T=T_0+\Delta T,$$

where T_0 is the initial uniform temperature $T_0=300K$ (where the plate is assumed to be stress free), and ΔT denotes the temperature change. Temperature change makes an initial deflection of the plate; thus, the natural frequency should be. Note that, in the cases studied, no buckling will arise due to thermal ambiance since the edges of the plate can move in-plane directions, so increasing the temperature will just yield a continuous deformation of the plate [53]. For nonlinear temperature rise, the temperature distribution along the thickness can be obtained by solving the following steady-state heat transfer equation by considering the boundary conditions through the thickness of the plate [18]:

$$\begin{aligned}
&-\frac{d}{dz}\left[\kappa(z)\frac{dT}{dz}\right]=0,\\
&\begin{cases} z=\dfrac{h}{2}\longrightarrow T=T_t,\\ z=-\dfrac{h}{2}\longrightarrow T=T_b,\end{cases}
\end{aligned}$$

in which T_t and T_b are the temperatures at top and bottom surfaces of the plate. The solution of this equation, by means of polynomial series, is:

$$T(z)=T_b+(T_t-T_b)\eta(z),$$

where

$$\begin{aligned}
\eta(z)=&\frac{1}{c}\Big[\Big(\frac{1}{2}+\frac{z}{h}\Big)-\frac{\kappa_{cm}}{(n+1)\kappa_m}\Big(\frac{1}{2}+\frac{z}{h}\Big)^{n+1}+\frac{\kappa_{cm}^2}{(2n+1)\kappa_m^2}\Big(\frac{1}{2}+\frac{z}{h}\Big)^{2n+1}\\
&-\frac{\kappa_{cm}^3}{(3n+1)\kappa_m^3}\Big(\frac{1}{2}+\frac{z}{h}\Big)^{3n+1}+\frac{\kappa_{cm}^4}{(4n+1)\kappa_m^4}\Big(\frac{1}{2}+\frac{z}{h}\Big)^{4n+1}\\
&-\frac{\kappa_{cm}^5}{(5n+1)\kappa_m^5}\Big(\frac{1}{2}+\frac{z}{h}\Big)^{5n+1}\Big],\\
C=1&-\frac{\kappa_{cm}}{(n+1)\kappa_m}+\frac{\kappa_{cm}^2}{(2n+1)\kappa_m^2}-\frac{\kappa_{cm}^3}{(3n+1)\kappa_m^3}+\frac{\kappa_{cm}^4}{(4n+1)\kappa_m^4}-\frac{\kappa_{cm}^5}{(5n+1)\kappa_m^5},\\
\kappa_{cm}=&\kappa_c-\kappa_m.
\end{aligned}$$

For linear temperature rise and isotropic plates (pure ceramic and pure metal), the temperature field will simply become as:

$$T(z)=T_b+(T_t-T_b)\Big(\frac{1}{2}+\frac{z}{h}\Big).$$

2.2 Governing equations and boundary conditions

The equivalent single layer laminated plate theories are developed by assuming the form of the displacement field as a linear function of the transverse dimension z. One of the equivalent single layer laminated plate theories is the FSDT, which is based on the displacement field: [54]:

$$\begin{aligned}
&u(x,y,z,t)=\bar{u}(x,y,z,t)+z\varphi_x(x,y,t),\\
&v(x,y,z,t)=\bar{v}(x,y,z,t)+z\varphi_y(x,y,t),\\
&w(x,y,z,t)=\bar{w}(x,y,z,t),
\end{aligned}$$

where $\bar{u}$, $\bar{v}$, and $\bar{w}$ denote the displacement components along the x, y and z coordinate directions, respectively, of a point on the midplane (i.e., $z=0$), φ_x and φ_y are the rotations about the y and x axis, respectively. For a small deformation, the square gradient of displacement can be omitted; But if the normal lateral rotation angle is in the average range, i.e., 10 to 15 degrees, the terms $(\frac{\partial w}{\partial x})^2$, $(\frac{\partial w}{\partial y})^2$, and $(\frac{\partial w}{\partial x})(\frac{\partial w}{\partial y})$ cannot be ignored. This induces geometrical nonlinearity, and the strains (ε) become nonlinear. By assuming large deformations, van Kármán's nonlinear displacement strain relations are expressed as follows [54]:

$$\varepsilon_{xx}=\frac{\partial u}{\partial x}+\frac{1}{2}\Big(\frac{\partial w}{\partial x}\Big)^2=\frac{\partial \bar{u}}{\partial x}+z\frac{\partial \varphi_x}{\partial x}+\frac{1}{2}\Big(\frac{\partial \bar{w}}{\partial x}\Big)^2,\ \ \varepsilon_{yy}=\frac{\partial v}{\partial y}+\frac{1}{2}\Big(\frac{\partial w}{\partial y}\Big)^2=\frac{\partial \bar{v}}{\partial y}+z\frac{\partial \varphi_y}{\partial y}+\frac{1}{2}\Big(\frac{\partial \bar{w}}{\partial y}\Big)^2, \tag{2.1a}$$

$$\varepsilon_{xy}=\frac{1}{2}\Big(\frac{\partial u}{\partial y}+\frac{\partial v}{\partial x}+\Big(\frac{\partial w}{\partial x}\Big)\Big(\frac{\partial w}{\partial y}\Big)\Big)=\frac{1}{2}\Big(\frac{\partial \bar{v}}{\partial x}+\frac{\partial \bar{u}}{\partial y}+z\Big(\frac{\partial \varphi_x}{\partial y}+\frac{\partial \varphi_y}{\partial x}\Big)+\Big(\frac{\partial \bar{w}}{\partial x}\Big)\Big(\frac{\partial \bar{w}}{\partial y}\Big)\Big), \tag{2.1b}$$

$$\varepsilon_{xz}=\frac{1}{2}\Big(\frac{\partial \bar{w}}{\partial x}+\varphi_x\Big),\quad \varepsilon_{yz}=\frac{1}{2}\Big(\frac{\partial \bar{w}}{\partial y}+\varphi_y\Big). \tag{2.1c}$$

The matrix form of Eq. (2.1) is as follows:

$$[\varepsilon]=\begin{bmatrix}\varepsilon_{xx}\\ \varepsilon_{yy}\\ \varepsilon_{xy}\\ \varepsilon_{xz}\\ \varepsilon_{yz}\end{bmatrix}=\begin{bmatrix}\frac{\partial \bar{u}}{\partial x}+\frac{1}{2}\Big(\frac{\partial \bar{w}}{\partial x}\Big)^2\\ \frac{\partial \bar{v}}{\partial y}+\frac{1}{2}\Big(\frac{\partial \bar{w}}{\partial y}\Big)^2\\ \frac{1}{2}\Big(\frac{\partial \bar{v}}{\partial x}+\frac{\partial \bar{u}}{\partial y}+\Big(\frac{\partial \bar{w}}{\partial x}\Big)\Big(\frac{\partial \bar{w}}{\partial y}\Big)\Big)\\ \frac{1}{2}\Big(\frac{\partial \bar{w}}{\partial x}+\varphi_x\Big)\\ \frac{1}{2}\Big(\frac{\partial \bar{w}}{\partial y}+\varphi_y\Big)\end{bmatrix}+z\begin{bmatrix}\frac{\partial \varphi_x}{\partial x}\\ \frac{\partial \varphi_y}{\partial y}\\ \frac{1}{2}\Big(\frac{\partial \varphi_x}{\partial y}\Big)\Big(\frac{\partial \varphi_y}{\partial x}\Big)\\ 0\\ 0\end{bmatrix}. \tag{2.2}$$

Hooke's law (stress-strain relations) for orthotropic FGM based on the FSDT can be shown below [55]:

$$\begin{Bmatrix} \sigma_{xx} \\ \sigma_{yy} \\ \tau_{yz} \\ \tau_{xz} \\ \tau_{xy} \end{Bmatrix} = \begin{bmatrix} C_{11} & C_{12} & 0 & 0 & 0 \\ C_{12} & C_{22} & 0 & 0 & 0 \\ 0 & 0 & C_{44} & 0 & 0 \\ 0 & 0 & 0 & C_{55} & 0 \\ 0 & 0 & 0 & 0 & C_{66} \end{bmatrix} \begin{Bmatrix} \varepsilon_{xx} \\ \varepsilon_{yy} \\ \gamma_{yz} \\ \gamma_{xz} \\ \gamma_{xy} \end{Bmatrix}, \tag{2.3}$$

where γ is the engineering strain and C_{ij} $(i,j=1-6)$ are the coefficients of the stiffness matrix, which are expressed as follows:

$$\begin{aligned} &C_{11}(z)=C_{22}(z)=\frac{E(z,T)}{1-\vartheta(z)^2}, \\ &C_{12}(z)=\frac{E(z,T)\vartheta(z)}{1-\vartheta(z)^2}, \\ &C_{44}(z)=C_{55}(z)=C_{66}(z)=\frac{E(z,T)}{2(1+\vartheta(z))}. \end{aligned}$$

2.3 Hamilton's principle

Hamilton's principle to achieve the governing equation is presented as follows:

$$\delta\int_0^T [U+W_1+W_2-K]dt=0, \tag{2.4}$$

where U, K, W_1 and W_2 are the strain energy of the system, the kinetic energy of the system, the work done by the external load q and the work done due to thermal effects, respectively. The variation of strain energy is displayed as follows:

$$\begin{aligned} \delta\int_{t_1}^{t_2} U dt = \int_{t_1}^{t_2}\int_S\int_{-\frac{h}{2}}^{\frac{h}{2}} \Big[&\sigma_{xx}\delta\varepsilon_{xx}+\sigma_{yy}\delta\varepsilon_{yy}+\sigma_{zz}\delta\varepsilon_{zz} \\ &+2(\sigma_{xy}\delta\varepsilon_{xy}+\sigma_{yz}\delta\varepsilon_{yz}+\sigma_{xz}\delta\varepsilon_{xz})\Big] dzdSdt, \end{aligned} \tag{2.5}$$

where S is the surface of the plate and $\delta\varepsilon_{zz}=0$. The kinetic energy is obtained as follows [56]:

$$K=\frac{1}{2}\int_V \rho(z)\Big(\frac{\partial u_i}{\partial t}\Big)^2 dV=\frac{1}{2}\int_S\int_{-\frac{h}{2}}^{\frac{h}{2}}\rho(z)\Big[\Big(\frac{\partial u}{\partial t}\Big)^2+\Big(\frac{\partial v}{\partial t}\Big)^2+\Big(\frac{\partial w}{\partial t}\Big)^2\Big]dzdS.$$

The variation of kinetic energy is obtained as follows [56]:

$$
\begin{aligned}
\delta K=\int_S\Big[&I_0\Big(\frac{\partial\bar{u}}{\partial t}\frac{\partial\delta\bar{u}}{\partial t}+\frac{\partial\bar{v}}{\partial t}\frac{\partial\delta\bar{v}}{\partial t}+\frac{\partial\bar{w}}{\partial t}\frac{\partial\delta\bar{w}}{\partial t}\Big)\\
&+I_1\Big(\frac{\partial\bar{u}}{\partial t}\frac{\partial\delta\varphi_x}{\partial t}+\frac{\partial\varphi_x}{\partial t}\frac{\partial\delta\bar{u}}{\partial t}+\frac{\partial\bar{v}}{\partial t}\frac{\partial\delta\varphi_y}{\partial t}+\frac{\partial\varphi_y}{\partial t}\frac{\partial\delta\bar{v}}{\partial t}\Big)\\
&+I_2\Big(\frac{\partial\varphi_x}{\partial t}\frac{\partial\delta\varphi_x}{\partial t}+\frac{\partial\varphi_y}{\partial t}\frac{\partial\delta\varphi_y}{\partial t}\Big)\Big]dS,
\end{aligned}
$$

which (I_2,I_1,I_0) are mass inertias defined by:

$$
(I_0,I_1,I_2)=\int_{-\frac{h}{2}}^{\frac{h}{2}}\rho(z)(1,z,z^2)dz.
$$

The variation of work done due to temperature changes is expressed as follows:

$$
\begin{aligned}
&\delta W_2=\int_S\Big[N_{xx}^T\frac{\partial\bar{w}}{\partial x}\frac{\partial\delta\bar{w}}{\partial x}+N_{xy}^T\frac{\partial\bar{w}}{\partial x}\frac{\partial\delta\bar{w}}{\partial y}+N_{yy}^T\frac{\partial\bar{w}}{\partial y}\frac{\partial\delta\bar{w}}{\partial y}\Big]dS,\\
&(N_{xx}^T,N_{yy}^T)=-\int_{-\frac{h}{2}}^{\frac{h}{2}}\Big(\alpha(z,T)\Delta T\frac{E(z,T)}{1-\vartheta(z)}\Big)dZ,\quad N_{xy}^T=0.
\end{aligned}
$$

The thermal load does not cause movement inside the plane and $\Delta T=T-T_0$ where T_0 is the initial temperature of the system, in which the plate is without tension. The variation work done by the external load is calculated as follows:

$$
\delta W_1=-\int q\delta\bar{w}dS. \tag{2.6}
$$

By putting the Eqs. (2.5)-(2.6) in the Eq. (2.4) and setting the displacement coefficients to zero according to the fundamental lemma of the calculus of variations, the Euler-Lagrange equation is obtained as follows [55]:

$$
\delta\bar{u}=\frac{\partial N_{xx}}{\partial x}+\frac{\partial N_{xy}}{\partial y}=I_0\frac{\partial^2\bar{u}}{\partial t^2}+I_1\frac{\partial^2\varphi_x}{\partial t^2}, \tag{2.7}
$$

$$
\delta\bar{v}=\frac{\partial N_{yy}}{\partial y}+\frac{\partial N_{xy}}{\partial x}=I_0\frac{\partial^2\bar{v}}{\partial t^2}+I_1\frac{\partial^2\varphi_y}{\partial t^2}, \tag{2.8}
$$

$$
\begin{aligned}
\delta\bar{w}=&\frac{\partial Q_x}{\partial x}+\frac{\partial Q_y}{\partial y}+\frac{\partial}{\partial x}\Big(N_{xx}\frac{\partial\bar{w}}{\partial x}+N_{xy}\frac{\partial\bar{w}}{\partial y}\Big)+\frac{\partial}{\partial y}\Big(N_{yy}\frac{\partial\bar{w}}{\partial y}+N_{xy}\frac{\partial\bar{w}}{\partial x}\Big)+N_{xx}^T\frac{\partial^2\bar{w}}{\partial x^2}\\
&+2N_{xy}^T\frac{\partial^2\bar{w}}{\partial x\partial y}+N_{yy}^T\frac{\partial^2\bar{w}}{\partial y^2}+q(x,y,t)=I_0\frac{\partial^2\bar{w}}{\partial t^2},
\end{aligned} \tag{2.9}
$$

$$
\delta\varphi_x:\frac{\partial M_{xx}}{\partial x}+\frac{\partial M_{xy}}{\partial y}-Q_x=I_2\frac{\partial^2\varphi_x}{\partial t^2}+I_1\frac{\partial^2\bar{u}}{\partial t^2}, \tag{2.10}
$$

$$
\delta\varphi_y:\frac{\partial M_{yy}}{\partial y}+\frac{\partial M_{xy}}{\partial x}-Q_y=I_2\frac{\partial^2\varphi_y}{\partial t^2}+I_1\frac{\partial^2\bar{v}}{\partial t^2}, \tag{2.11}
$$

where N_{ij}, M_{ij}, and Q_{ij} are the stress resultants defined by:

$$\left\{\begin{array}{c} N_{xx} \\ N_{yy} \\ N_{xy} \end{array}\right\} = \int_{-\frac{h}{2}}^{\frac{h}{2}} \left\{\begin{array}{c} \sigma_{xx} \\ \sigma_{yy} \\ \tau_{xy} \end{array}\right\} dz, \quad \left\{\begin{array}{c} M_{xx} \\ M_{yy} \\ M_{xy} \end{array}\right\} = \int_{-\frac{h}{2}}^{\frac{h}{2}} z \left\{\begin{array}{c} \sigma_{xx} \\ \sigma_{yy} \\ \tau_{xy} \end{array}\right\} dz, \tag{2.12}$$

$$\left\{\begin{array}{c} Q_x \\ Q_y \end{array}\right\} = \int_{-\frac{h}{2}}^{\frac{h}{2}} K \left\{\begin{array}{c} \tau_{xz} \\ \tau_{yz} \end{array}\right\} dz, \tag{2.13}$$

where K is the shear correction factor, which can be anticipated to be a function of z and given by [57]:

$$K = \frac{5}{6-(\vartheta_c V_c(z)+\vartheta_m V_m(z)))}. \tag{2.14}$$

By putting Eq. (2.2) in (2.3) and then by putting in Eqs. (2.7) and (2.12), the following equations are obtained [54]:

$$\begin{aligned}
&A_{11}\Big(\frac{\partial^2 \bar{u}}{\partial x^2}+\frac{\partial^2 \bar{w}}{\partial x}\frac{\partial^2 \bar{w}}{\partial x^2}\Big)+A_{12}\Big(\frac{\partial^2 \bar{v}}{\partial x \partial y}+\frac{\partial^2 \bar{w}}{\partial y}\frac{\partial^2 \bar{w}}{\partial x \partial y}\Big)+B_{11}\frac{\partial^2 \varphi_x}{\partial x^2}+B_{12}\frac{\partial^2 \varphi_y}{\partial x \partial y} \\
&\quad +A_{66}\Big(\frac{\partial^2 \bar{u}}{\partial y^2}+\frac{\partial^2 \bar{v}}{\partial x \partial y}+\frac{\partial \bar{w}}{\partial y}\frac{\partial^2 \bar{w}}{\partial x \partial y}+\frac{\partial \bar{w}}{\partial x}\frac{\partial^2 \bar{w}}{\partial y^2}\Big)+B_{66}\Big(\frac{\partial^2 \varphi_x}{\partial y^2}+\frac{\partial^2 \varphi_y}{\partial x \partial y}\Big) \\
&=I_0\frac{\partial^2 \bar{u}}{\partial t^2}+I_1\frac{\partial^2 \varphi_x}{\partial t^2},
\end{aligned} \tag{2.15}$$

$$\begin{aligned}
&A_{66}\Big(\frac{\partial^2 \bar{u}}{\partial x \partial y}+\frac{\partial^2 \bar{v}}{\partial x^2}+\frac{\partial \bar{w}}{\partial y}\frac{\partial^2 \bar{w}}{\partial x^2}+\frac{\partial \bar{w}}{\partial x}\frac{\partial^2 \bar{w}}{\partial x \partial y}\Big)+B_{66}\Big(\frac{\partial^2 \varphi_y}{\partial x^2}+\frac{\partial^2 \varphi_x}{\partial x \partial y}\Big) \\
&\quad +A_{12}\Big(\frac{\partial^2 \bar{u}}{\partial x \partial y}+\frac{\partial \bar{w}}{\partial x}\frac{\partial^2 \bar{w}}{\partial x \partial y}\Big)+A_{22}\Big(\frac{\partial^2 \bar{v}}{\partial y^2}+\frac{\partial \bar{w}}{\partial y}\frac{\partial^2 \bar{u}}{\partial y^2}\Big)+B_{12}\frac{\partial^2 \varphi_x}{\partial x \partial y}+B_{22}\frac{\partial^2 \varphi_y}{\partial y^2} \\
&=I_0\frac{\partial^2 \bar{v}}{\partial t^2}+I_1\frac{\partial^2 \varphi_y}{\partial t^2},
\end{aligned} \tag{2.16}$$

$$\begin{aligned}
&KA_{55}\Big(\frac{\partial^2 \bar{w}}{\partial x^2}+\frac{\partial \varphi_x}{\partial x}\Big)+KA_{44}\Big(\frac{\partial^2 \bar{w}}{\partial y^2}+\frac{\partial \varphi_y}{\partial y}\Big)+\frac{\partial \bar{w}}{\partial x}\Bigg(A_{11}\Big(\frac{\partial^2 \bar{u}}{\partial x^2}+\frac{\partial \bar{w}}{\partial x}\frac{\partial^2 \bar{w}}{\partial x^2}\Big) \\
&\quad +B_{11}\frac{\partial^2 \varphi_x}{\partial x^2}+A_{12}\Big(\frac{\partial^2 \bar{v}}{\partial x \partial y}+\frac{\partial^2 \bar{w}}{\partial y}\frac{\partial^2 \bar{w}}{\partial x \partial y}\Big)+B_{12}\frac{\partial^2 \varphi_y}{\partial x \partial y}\Bigg)+\frac{\partial^2 \bar{w}}{\partial x^2}\Bigg(A_{11}\Big(\frac{\partial \bar{u}}{\partial x}+\frac{1}{2}\Big(\frac{\partial \bar{w}}{\partial x}\Big)^2\Big) \\
&\quad +B_{11}\frac{\partial \varphi_x}{\partial x}+A_{12}\Big(\frac{\partial \bar{v}}{\partial y}+\frac{1}{2}\Big(\frac{\partial \bar{w}}{\partial y}\Big)^2\Big)+B_{12}\frac{\partial \varphi_y}{\partial y}\Bigg)+2\frac{\partial^2 \bar{w}}{\partial x \partial y}\Bigg(A_{66}\Big(\frac{\partial \bar{u}}{\partial y}+\frac{\partial \bar{v}}{\partial x}+\frac{\partial \bar{w}}{\partial y}\frac{\partial \bar{w}}{\partial x}\Big) \\
&\quad +B_{66}\Big(\frac{\partial \varphi_x}{\partial y}+\frac{\partial \varphi_y}{\partial x}\Big)\Bigg)+\frac{\partial \bar{w}}{\partial y}\Bigg(A_{66}\Big(\frac{\partial^2 \bar{u}}{\partial x \partial y}+\frac{\partial^2 \bar{v}}{\partial x^2}+\frac{\partial \bar{w}}{\partial y}\frac{\partial^2 \bar{w}}{\partial y \partial x^2}\Big)+B_{66}\Big(\frac{\partial^2 \varphi_x}{\partial x \partial y}+\frac{\partial^2 \varphi_y}{\partial x^2}\Big)\Bigg) \\
&\quad +\frac{\partial \bar{w}}{\partial x}\Bigg(A_{66}\Big(\frac{\partial \bar{u}}{\partial y^2}+\frac{\partial^2 \bar{v}}{\partial x \partial y}+\frac{\partial \bar{w}}{\partial y}\frac{\partial^2 \bar{w}}{\partial x \partial y}+\frac{\partial \bar{w}}{\partial x}\frac{\partial^2 \bar{w}}{\partial y^2}\Big)++B_{66}\Big(\frac{\partial^2 \varphi_x}{\partial y^2}+\frac{\partial^2 \varphi_y}{\partial x \partial y}\Big)\Bigg)
\end{aligned}$$

$$
\begin{aligned}
&+\frac{\partial^2\partial\bar{w}}{\partial y^2}\left(A_{12}\Big(\frac{\partial\bar{u}}{\partial x}+\frac{1}{2}\Big(\frac{\partial\bar{w}}{\partial x}\Big)^2\Big)+B_{12}\frac{\partial\varphi_x}{\partial x}+A_{22}\Big(\frac{\partial\bar{v}}{\partial y}+\frac{1}{2}\Big(\frac{\partial\bar{w}}{\partial y}\Big)^2\Big)+B_{22}\frac{\partial\varphi_y}{\partial y}\right)\\
&+\frac{\partial\bar{w}}{\partial y}\left(A_{22}\Big(\frac{\partial^2\bar{v}}{\partial y^2}+\frac{\partial\bar{w}}{\partial y}\frac{\partial^2\bar{w}}{\partial y^2}\Big)+B_{22}\frac{\partial^2\varphi_y}{\partial y^2}+A_{12}\Big(\frac{\partial^2\bar{u}}{\partial x\partial y}+\frac{\partial\bar{w}}{\partial x}\frac{\partial^2\bar{w}}{\partial x\partial y}\Big)+B_{12}\frac{\partial^2\varphi_x}{\partial x\partial y}\right)\\
&+N_{xx}^T\frac{\partial^2\bar{w}}{\partial x^2}+2N_{xy}^T\frac{\partial^2\bar{w}}{\partial x\partial y}+N_{yy}^T\frac{\partial^2\bar{w}}{\partial y^2}+q(x,y,t)=I_0\frac{\partial^2\bar{w}}{\partial t^2},
\end{aligned}
\tag{2.17}
$$

$$
\begin{aligned}
&B_{11}\Big(\frac{\partial^2\bar{u}}{\partial x^2}+\frac{\partial\bar{w}}{\partial x}\frac{\partial^2\bar{w}}{\partial x^2}\Big)+D_{11}\frac{\partial^2\varphi_x}{\partial x^2}+B_{12}\Big(\frac{\partial^2\bar{v}}{\partial x\partial y}+\frac{\partial\bar{w}}{\partial y}\frac{\partial^2\bar{w}}{\partial x\partial y}\Big)+D_{12}\frac{\partial^2\varphi_y}{\partial x\partial y}\\
&\quad+B_{66}\Big(\frac{\partial^2\bar{u}}{\partial y^2}+\frac{\partial^2\bar{v}}{\partial x\partial y}+\frac{\partial\bar{w}}{\partial y}\frac{\partial^2\bar{w}}{\partial x\partial y}+\frac{\partial\bar{w}}{\partial x}\frac{\partial^2\bar{w}}{\partial y^2}\Big)+D_{66}\Big(\frac{\partial^2\varphi_x}{\partial y^2}+\frac{\partial^2\varphi_y}{\partial x\partial y}\Big)-KA_{55}\Big(\frac{\partial\bar{w}}{\partial x}+\varphi_x\Big)\\
&=I_2\frac{\partial^2\varphi_x}{\partial t^2}+I_1\frac{\partial^2\bar{u}}{\partial t^2},
\end{aligned}
\tag{2.18}
$$

$$
\begin{aligned}
&B_{66}\Big(\frac{\partial^2\bar{v}}{\partial x^2}+\frac{\partial^2\bar{u}}{\partial x\partial y}+\frac{\partial\bar{w}}{\partial x}\frac{\partial^2\bar{w}}{\partial x\partial y}+\frac{\partial\bar{w}}{\partial y}\frac{\partial^2\bar{w}}{\partial x^2}\Big)+D_{66}\Big(\frac{\partial^2\varphi_y}{\partial x^2}+\frac{\partial^2\varphi_x}{\partial x\partial y}\Big)\\
&\quad+B_{12}\Big(\frac{\partial^2\bar{u}}{\partial x\partial y}+\frac{\partial\bar{w}}{\partial x}\frac{\partial^2\bar{w}}{\partial x\partial y}\Big)+B_{22}\Big(\frac{\partial^2\bar{v}}{\partial y^2}+\frac{\partial\bar{w}}{\partial y}\frac{\partial^2\bar{u}}{\partial y^2}\Big)+D_{12}\frac{\partial^2\varphi_x}{\partial x\partial y}+D_{22}\frac{\partial^2\varphi_y}{\partial y^2}-KA_{44}\Big(\frac{\partial\bar{w}}{\partial y}+\varphi^y\Big)\\
&=I_2\frac{\partial^2\varphi_y}{\partial t^2}+I_1\frac{\partial^2\bar{v}}{\partial t^2},
\end{aligned}
\tag{2.19}
$$

where A_{ij} are called extensional stiffnesses, D_{ij} the bending stiffnesses, and B_{ij} the bending-extensional coupling stiffnesses, which are defined in terms of the stiffness matrix as:

$$
(A_{ij},B_{ij},D_{ij})=\int_{-\frac{h}{2}}^{\frac{h}{2}}C_{ij}(z)(1,z,z^2)dz.
$$

Ignoring the plane moment of inertia in the above equations, I_1 and I_2 become zero. Considering the simply supported boundary conditions without plane displacement, the following relationships are established:

$$
\begin{aligned}
&\text{at } x=0,l_a, \qquad \bar{v}=\bar{w}=N_{xx}=M_{xx}=\varphi_y=0,\\
&\text{at } y=0,l_a, \qquad \bar{u}=\bar{w}=N_{yy}=M_{yy}=\varphi_y=0.
\end{aligned}
$$

The following displacement functions are defined to satisfy the boundary conditions [7]:

$$
\bar{u}(x,y,t)=\sum_{n=1}^{\infty}\sum_{m=1}^{\infty}U_{mm}(t)\cos(\alpha x)\sin(\beta y), \tag{2.20}
$$

$$
\bar{v}(x,y,t)=\sum_{n=1}^{\infty}\sum_{m=1}^{\infty}V_{mn}(t)\sin(\alpha x)\cos(\beta y), \tag{2.21}
$$

$$
\bar{w}(x,y,t)=\sum_{n=1}^{\infty}\sum_{m=1}^{\infty}W_{mn}(t)\sin(\alpha x)\sin(\beta y), \tag{2.22}
$$

$$\varphi_x(x,y,t)=\sum_{n=1}^{\infty}\sum_{m=1}^{\infty}X_{mn}(t)\cos(\alpha x)\sin(\beta y), \tag{2.23}$$

$$\varphi_y(x,y,t)=\sum_{n=1}^{\infty}\sum_{m=1}^{\infty}Y_{mn}(t)\sin(\alpha x)\cos(\beta y). \tag{2.24}$$

In the above relations, U, V, W, X and Y are the unknown time terms, $\beta=\frac{n\pi}{l_b}$, $\alpha=\frac{m\pi}{l_a}$ also m and n are half-wave numbers.

2.4 Specifications of sound pressure

The sound pressure that hits the FGM obliquely is assumed as follows [58]:

$$p_i(x,y,t)=P_i e^{i\bar{\Omega}t}e^{-i(k_x x+k_y y-k_z z)}, \tag{2.25}$$

where P_i is the incident sound pressure amplitude, $\bar{\Omega}$ is the incident frequency, $k_x=k\sin(\theta_i)\cos(\Phi_i)$, $k_y=k\sin(\theta_i)\cos(\Phi_i)$ and $k_z=k\cos(\theta_i)$ are the components of the wave vector which must satisfy the condition $k_x^2+k_y^2+k_z^2=k^2$, k is the wave number which is equal to $\frac{\bar{\Omega}}{c}$, where c is the speed of sound, θ_i is the incident angle and Φ_i is the azimuthal angle. Likewise, the waves reflected and transmitted from and through the plate can be signified as:

$$p_r(x,y,t)=P_r e^{i\bar{\Omega}t}e^{-i(k_x x+k_y y+k_z z)}, \tag{2.26}$$

$$p_t(x,y,t)=P_t e^{i\bar{\Omega}t}e^{-i(k_x x+k_y y-k_z z)}, \tag{2.27}$$

where P_r and P_t are the indefinite compound amplitudes of the reflected and transmitted waves, respectively [58]. Moreover, assuming that the panel is not made of porous material, the airspeed on each side of the panel is equal to the speed of the panel. By writing the Euler equation on both sides of the panel, the relations between pressure and transverse displacement can be conveyed as [58]:

$$-\frac{\partial(p_i+p_r)}{\partial z}=\rho_0\frac{\partial^2 w}{\partial t^2} \qquad \text{at } z=0, \tag{2.28}$$

$$-\frac{\partial(p_t)}{\partial z}=\rho_0\frac{\partial^2 w}{\partial t^2} \qquad \text{at } z=0, \tag{2.29}$$

where ρ_0 is the air density. Substituting, Eqs. (2.22), (2.25) and (2.26) into Eq. (2.28) and applying the Galerkin method with suitable weighting function, $\sin(\alpha x)\sin(\beta y)$, variable P_r is obtained in terms of P_i and $\frac{d^2 w_{mn}(t)}{dt^2}$ which is given in Appendix A. Similarly, substituting Eqs. (2.22) and (2.27) into Eq. (2.29) and using the Galerkin method with weighting function $\sin(\alpha x)\sin(\beta y)$, variable P_t is obtained in term of $\frac{d^2 w_{mn}(t)}{dt^2}$ which is given in Appendix A. External sound pressure is assumed in the plate motion equations as an external load:

$$q(x,y,t)=p_i(x,y,t)+p_r(x,y,t)-p_t(x,y,t). \tag{2.30}$$

In this investigation, the vibration in the first mode is examined. For this purpose, by putting $m=n=1$ in the Eqs. (2.20)-(2.24) and inserting them in the equations of motion (2.15)-(2.19) and applying the Galerkin method, the equations of motion are extracted as follows:

$$\Pi_{11}W^2-\Pi_{12}U-\Pi_{13}V-\Pi_{14}X-\Pi_{15}Y=0, \tag{2.31}$$

$$\Pi_{21}W^2-\Pi_{22}U-\Pi_{23}V-\Pi_{24}X-\Pi_{25}Y=0, \tag{2.32}$$

$$\Pi_{41}W^2-\Pi_{42}W-\Pi_{43}U-\Pi_{44}V-\Pi_{45}X-\Pi_{46}Y=0, \tag{2.33}$$

$$\Pi_{51}W^2-\Pi_{52}W-\Pi_{53}U-\Pi_{54}V-\Pi_{55}X-\Pi_{56}Y=0, \tag{2.34}$$

$$\begin{aligned} &I_0\frac{d^2W}{dt^2}+(-\Pi_{35}U-\Pi_{36}V+\Pi_{32})W+\Pi_{31}W^3+(-\Pi_{37}W+\Pi_{33})X \\ &\quad+(-\Pi_{38}W+C_{34})Y+\Pi_{39}\cos(\bar{\Omega}t+\phi)=0. \end{aligned} \tag{2.35}$$

The coefficients Π_{ij} and ϕ in the above equations depend on the geometry and properties of the plate, which are given in Appendix B. From the four Eqs. (2.31)-(2.34), the four unknowns, U,V,X and Y are obtained in terms of and by substituting in the Eq. (2.35), the following equation is derived:

$$\frac{d^2W}{dt^2}+\overline{a_1}\overline{W}+\overline{a_2}\overline{W}^2+\overline{a_3}\overline{W}^3+a_0\cos(\overline{\Omega}t+\phi)=0.$$

To simplify the solution, the dimensionless form of the above equation is derived as follows:

$$\frac{d^2W}{dT^2}+a_1W+a_2W^2+a_3W^3+a_0\cos(\Omega T+\phi)=0, \tag{2.36}$$

using the following dimensionless parameters:

$$W=\frac{\overline{W}}{h},\quad T=\frac{t}{h}\sqrt{\frac{E_m}{\rho_m}},\quad \omega=\overline{\Omega}h\sqrt{\frac{\rho_m}{E_m}}.$$

The coefficients a_i in the Eq. (2.36) are given in Appendix C.

3 Applying the HAM to the equation of motion

Now, we consider the equation of motion in a simply supported FG plate as:

$$\frac{d^2W}{dT^2}+a_1W(T)+a_2W^2(T)^2+a_3W^3(T)^3+a_0\cos(\omega T+\phi)=0, \tag{3.1}$$

$$W(0)=A,\quad \dot{W}(0)=0. \tag{3.2}$$

Under the transformation, $\tau=\Omega_q T$, Eq. (3.1) is converted to

$$\Omega_q^2\frac{\partial^2 W(\tau)}{d\tau^2}+a_1W(\tau)+a_2W(\tau)^2+a_3W(\tau)^3+a_0\cos\Big(\frac{\omega}{\Omega_q}\tau+\phi\Big)=0, \tag{3.3}$$

$$W(0)=A, \quad \dot{W}(0)=0, \tag{3.4}$$

in which Ω_q is the nonlinear frequency of vibration and is defined as

$$\Omega_q=\sum_{i=0}^{n}q^i\omega_i. \tag{3.5}$$

To solve Eq. (3.3) using the HAM, we choose $W_0(\tau)=A\cos(\tau)$ as the initial guess and

$$\mathcal{L}[\phi(\tau;q)]=\omega_0^2\Big[\frac{\partial^2\phi(\tau;q)}{\partial\tau^2}+\phi(\tau;q)\Big] \tag{3.6}$$

as the linear operator. From Eq. (3.3), we define

$$\mathcal{N}[\phi(\tau;q),\Omega_q]=\Omega_q^2\frac{\partial^2\phi(\tau;q)}{\partial\tau^2}+a_1\phi(\tau;q)+a_2\phi(\tau;q)^2+a_3\phi(\tau;q)^3+a_0\cos\Big(\frac{\omega}{\Omega_q}\tau+\phi\Big) \tag{3.7}$$

as the nonlinear operator. Now, one can create the following zeroth-order deformation equation

$$\begin{aligned}(1-q)\mathcal{L}[\phi(\tau;q)]=qk\Big[\Omega_q^2\frac{\partial^2\phi(\tau;q)}{\partial\tau^2}+a_1\phi(\tau;q)+a_2\phi(\tau;q)^2\\ +a_3\phi(\tau;q)^3+a_0\cos\Big(\frac{\omega}{\Omega_q}\tau+\phi\Big)\Big]\end{aligned} \tag{3.8}$$

with the initial conditions

$$\phi(0;q)=A, \quad \dot{\phi}(0;q)=0. \tag{3.9}$$

Expanding $\phi(0;q)$ in the Taylor series concerning the embedding parameter q gives

$$\phi(0;q)=W_0(\tau)+\sum_{m=1}^{+\infty}W_m(\tau)q^m. \tag{3.10}$$

Differentiating the zeroth-order deformation Eq. (3.8) and the initial conditions Eq. (3.9) m times ($m\geq 1$) concerning q and then setting $q=0$ and finally dividing them by $m!$ one can obtain

$$\begin{aligned}
&-\omega_0^2\Big(\frac{\partial^2 W_0(\tau)}{\partial\tau^2}\Big)-\omega_0^2W_0(\tau)-k\omega_0^2\Big(\frac{\partial^2 W_0(\tau)}{\partial\tau^2}\Big)-ka_1W_0(\tau)-ka_2W_0(\tau)^2\\
&\quad -ka_3W_0(\tau)^3+\omega_0^2\Big(\frac{\partial^2 W_1(\tau)}{\partial\tau^2}\Big)+\omega_0^2W_1(\tau)-ka_0\cos\Big(\frac{\omega}{\omega_0}\tau+\phi\Big)=0, \qquad (3.11)\\
&W_1(0)=0, \quad \dot{W}_1(0)=0, \qquad (3.12)\\
&-k\omega_0^2\Big(\frac{\partial^2 W_1(\tau)}{\partial\tau^2}\Big)-2ka_2W_0(\tau)W_1(\tau)-3ka_3W_0(\tau)^2W_1(\tau)-ka_1W_1(\tau)\\
&\quad -\frac{ka_0\sin\Big(\frac{\omega}{\omega_0}\tau+\phi\Big)\omega\tau\omega_1}{\omega_0^2}+\omega_0^2\Big(\frac{\partial^2 W_0(\tau)}{\partial\tau^2}\Big)+\omega_0^2W_2(\tau)\\
&\quad -\omega_0^2\Big(\frac{\partial^2 W_1(\tau)}{\partial\tau^2}\Big)-\omega_0^2W_1(\tau)-2k\Big(\frac{\partial^2 W_0(\tau)}{\partial\tau^2}\Big)\omega_0\omega_1=0, \qquad (3.13)\\
&W_2(0)=0, \quad \dot{W}_2(0)=0. \qquad (3.14)
\end{aligned}$$

Higher powers can be used if needed. Replacing the initial guess $W_0(\tau)=A\cos(\tau)$ into Eq. (3.11) gives

$$\begin{aligned}
&\Big(k\omega_0^2A-ka_1A-\frac{3}{4}ka_3A^3\Big)\cos(\tau)-\frac{1}{2}kA^2a_2\cos(2\tau)-\frac{1}{4}ka_3A^3\cos(3\tau)-\frac{1}{2}ka_2A^2\\
&\quad +\omega_0^2\Big(\frac{\partial^2 W_1(\tau)}{\partial\tau^2}\Big)+\omega_0^2W_1(\tau)-ka_0\cos\Big(\frac{\omega}{\omega_0}\tau+\phi\Big). \qquad (3.15)
\end{aligned}$$

Secular term causes dispersion of the answer and should be removed. At the same time, the nonlinear frequency is extracted from it. To eliminate the secular term in the first-order approximation, we set the coefficient of $\cos(\tau)$ in Eq. (3.15) equal to zero. This yield

$$\omega_0=\frac{1}{2}\sqrt{(3A^2a_3+4a_1)} \qquad (3.16)$$

and therefore

$$\begin{aligned}
&W_1(\tau)\\
&=\Big(\frac{9A^5a_3^2k-96A^4ka_2a_3-12A^3\omega^2a_3k+12A^3a_1a_3k+128A^2\omega^2a_2k-288A^2a_0a_3k-128A^2a_1a_2k-384a_1a_0k}{216A^4a_3^2-288A^2\omega^2a_3+576A^2a_1a_3-384\omega^2a_1+384a_1^2}\Big)\cos(\tau)\\
&\quad+\Big(\frac{-48A^4ka_2a_3+64A^2\omega^2a_2k-64A^2a_1a_2k}{216A^4a_3^2-288A^2\omega^2a_3+576A^2a_1a_3-384\omega^2a_1+384a_1^2}\Big)\cos(2\tau)\\
&\quad+\Big(\frac{-9A^5a_3^2k+12A^3\omega^2a_3k-12A^3a_1a_3k}{216A^4a_3^2-288A^2\omega^2a_3+576A^2a_1a_3-384\omega^2a_1+384a_1^2}\Big)\cos(3\tau)\\
&\quad+\Big(\frac{288A^2a_0a_3k+384a_1a_0k}{216A^4a_3^2-288A^2\omega^2a_3+576A^2a_1a_3-384\omega^2a_1+384a_1^2}\Big)\cos\Big(\frac{2\omega\tau}{\sqrt{3A^2a_3+4a_1}}+\phi\Big)\\
&\quad+\Big(\frac{144A^4ka_2a_3-192A^2\omega^2a_2k+192A^2a_1a_2k}{216A^4a_3^2-288A^2\omega^2a_3+576A^2a_1a_3-384\omega^2a_1+384a_1^2}\Big). \qquad (3.17)
\end{aligned}$$

Similarly, we find

$$
\begin{aligned}
\omega_1 = &\frac{1}{96}\frac{Ak}{\sqrt{3A^2a_3+4a_1}(9A^4a_3^2-12A^2\omega^2a_3+24A^2a_1a_3-16\omega^2a_1+16a_1^2)}\Big(27A^5a_3^2-576A^4a_2a_3^2\\
&-36A^3\omega^2a_3^2+36A^3a_1a_3^2+960A^3a_2^2a_3+768A^2\omega^2a_2a_3-1728A^2a_3^2a_0-768A^2a_1a_2a_3\\
&-1280A\omega^2a_2^2+1280Aa_1a_2^2-2304a_0a_1a_3\Big).
\end{aligned}
\tag{3.18}
$$

Now, fundamental nonlinear frequency-amplitude relation and deflection-time and amplitude relation for vibrating actuated simply supported FG plate can be estimated as below

$$
\begin{aligned}
\Omega\equiv\Omega_q\cong&\,\omega_0+\omega_1=\frac{1}{2}\sqrt{(3A^2a_3+4a_1)}\\
&+\frac{1}{96}\frac{Ak}{\sqrt{3A^2a_3+4a_1}(9A^4a_3^2-12A^2\omega^2a_3+24A^2a_1a_3-16\omega^2a_1+16a_1^2)}\Big(27A^5a_3^2-576A^4a_2a_3^2\\
&-36A^3\omega^2a_3^2+36A^3a_1a_3^2+960A^3a_2^2a_3+768A^2\omega^2a_2a_3-1728A^2a_3^2a_0-768A^2a_1a_2a_3\\
&-1280A\omega^2a_2^2+1280Aa_1a_2^2-2304a_0a_1a_3\Big)
\end{aligned}
\tag{3.19}
$$

and

$$
\begin{aligned}
&W(\tau)\cong W_0(\tau)+W_1(\tau)=\Bigg(A\\
&+\frac{9A^5a_3^2k-96A^4ka_2a_3-12A^3\omega^2a_3k+12A^3a_1a_3k+128A^2\omega^2a_2k-288A^2a_0a_3k-128A^2a_1a_2k-384a_1a_0k}{216A^4a_3^2-288A^2\omega^2a_3+576A^2a_1a_3-384\omega^2a_1+384a_1^2}\Bigg)\cos(\tau)\\
&+\left(\frac{-48A^4ka_2a_3+64A^2\omega^2a_2k-64A^2a_1a_2k}{216A^4a_3^2-288A^2\omega^2a_3+576A^2a_1a_3-384\omega^2a_1+384a_1^2}\right)\cos(2\tau)\\
&+\left(\frac{-9A^5a_3^2k+12A^3\omega^2a_3k-12A^3a_1a_3k}{216A^4a_3^2-288A^2\omega^2a_3+576A^2a_1a_3-384\omega^2a_1+384a_1^2}\right)\cos(3\tau)\\
&+\left(\frac{288A^2a_0a_3k+384a_1a_0k}{216A^4a_3^2-288A^2\omega^2a_3+576A^2a_1a_3-384\omega^2a_1+384a_1^2}\right)\cos\Big(\frac{2\omega\tau}{\sqrt{3A^2a_3+4a_1}}+\phi\Big)\\
&+\left(\frac{144A^4ka_2a_3-192A^2\omega^2a_2k+192A^2a_1a_2k}{216A^4a_3^2-288A^2\omega^2a_3+576A^2a_1a_3-384\omega^2a_1+384a_1^2}\right).
\end{aligned}
\tag{3.20}
$$

224 # 4 Modeling the vibroacoustic response of FG plate

In this section, an acoustic model is considered to calculate the free field sound radiation associated with a given vibration response. The vibration response of the FG plate in terms of displacement and velocity is resolute by applying the transmitted sound pressure of the plate $p_t(x,y,t)$ obtained from Section 2. Fluid-structure interaction is not involved in the present model. Acoustic wave propagation through a light homogeneous elastic fluid such as air, for which the fluid-structure interaction can be ignored, is defined by the wave equation. The time average of the sound intensity is obtained from [30]:

$$\bar{I}=\frac{1}{2}Real(p_t\dot{w}^*), \tag{4.1}$$

where $\dot{w}^*$ is the speed of the sound particle and the superscript $*$ indicates the complex conjugate. The sound power produced in a certain volume is identical to the surface integral of the normal constituent of the sound intensity as:

$$\overline{W}=\oint \bar{I}\cdot ndS, \tag{4.2}$$

where n is the surface normal. If the surface utilized to evaluate this countenance is chosen to be equal to the surface of the introduced vibrating plate, the sound power can be written as follows:

$$\overline{W}=\frac{1}{2}Real\Big(\oint p_t\dot{w}^*dS\Big). \tag{4.3}$$

The above equation can be written in decibel scale as follows:

$$SPL=10\log\Big(\frac{\overline{W}}{\overline{W}_{ref}}\Big)=20\log\Big(\frac{p}{p_{ref}}\Big), \tag{4.4}$$

where $\overline{W}_{ref}$ is the power of the sound source which is equal to $10^{-12}(W)$, andp_{ref} is the pressure of the sound source which is equal to $20\times10^{-6}(Pa)$ [31]. Radiation efficiency is a quantity to know how a vibrating object radiates sound [31], which is distinct as the ratio of the sound power radiated per surface unit by the object to the sound power radiated per surface unit by the sound source, as follows:

$$\sigma=\frac{\overline{W}}{\rho_0c_0S\langle\overline{\dot{W}}^2\rangle}, \tag{4.5}$$

where $\langle\overline{\dot{W}}^2\rangle=\frac{1}{8}\dot{W}^2$ is the average mean square velocity of the plate and c_0 is the sound speed [31]. Sound transmission loss is the ratio of incident sound power to transmitted sound power. The sound transmission loss in decibels is as follows [1]:

$$STL=10\log\Big(\frac{1}{\tau}\Big), \tag{4.6}$$

where τ is the transmission coefficient, which is defined as the ratio of transmission power and incident power $\left(\frac{\overline{W}_t}{\overline{W}_I}\right)$. Since the incident sound wave is a plane wave, its intensity is $\frac{p_i^2}{2\rho_0 c_0}$. The incident intensity on the plane is the intensity value that is perpendicular to the plane. Therefore, the incident intensity is equal to [1]:

$$I_i = \frac{\rho_i^2 \cos\theta_i}{2\rho_0 c_0}.$$

Incident sound power $\overline{W_l}$ is simply achieved by multiplying the intensity of the incident by the area of the plate, in the area it affects [30]:

$$\overline{W_l} = \frac{p_i^2 S \cos\theta_i}{2\rho_0 c_0}.$$

Transmitted sound power can be defined as follows [30]:

$$\overline{W_t} = \frac{1}{2} Real\Big(\oint p_t \dot{w}^* dS \Big).$$

The above integral can be solved numerically using Simpson's one-third rule.

5 Results and discussions

In this section, selected numerical results are obtainable and compared with the previous literature to analyze the effects of different parameters on the nonlinear natural frequencies and acoustic responses of the FG plates. Two sets of material mixtures are considered. One is aluminum and alumina, referred to as Al/Al_2O_3 and the other is stainless steel and silicon nitride, referred to as $SUS304/Si_3N_4$. The upper surface of these FG plates is ceramic-rich and the lower surface is metal-rich. The properties of Al/Al_2O_3 rectangular FG plates which are temperature-independent, $E_m = 70\times 10^9 (Pa)$, $E_c = 380\times 10^9 (Pa)$, $\rho_m = 2707(\frac{kg}{m^3})$, $\rho_c = 3800(\frac{kg}{m^3})$, $\alpha_m = 23\times 10^{-6}(\frac{1}{c})$, $\alpha_c = 7.4\times 10^{-6}(\frac{1}{c})$, $\kappa_m = 204(\frac{W}{mk})$, $\kappa_c = 10.4(\frac{W}{mk})$ and $\vartheta_m = \vartheta_c = 0.3$ [18]. For Si_3N_4, the mass density is: $\rho_c = 2370\left(\frac{kg}{m^3}\right)$, and for $SUS304$ is: $\rho_m = 8166\left(\frac{kg}{m^3}\right)$. Young's modulus, thermal expansion coefficients, thermal conductivities and Poisson's ratios of $SUS304/Si_3N_4$, which are assumed to be temperature-dependent, listed in Table 1 [18,59]:

Table 2 shows the fundamental frequency of Al/Al_2O_3 square FG plate. Table 2 also includes the results presented by [12, 53]. The frequency parameters are in complete agreement with these references, which validates the linear part of the present model.

In Table 3, the nonlinear frequency ratio $\left(\frac{\omega_{NL}}{\omega_L}\right)$ of free vibration on Al/Al_2O_3 square FG plate for different values of the index and non-dimensional amplitude A has been extracted and compared with the results of the references [7,10]. As can be seen in Table 3, the results have good accuracy. In the reference [10], the author has used CPT, whereas in the present research, FSDT is used, and shear effects are considered; as a result, the

Table 1: Temperature-dependent coefficients of material properties for $SUS304/Si_3N_4$.

Parameter	Material	P_{-1}	P_0	P_1	P_2	P_3
E(Pa)	Si_3N_4	0	348.43×10^{9}	-3.070×10^{-4}	2.160×10^{-7}	-8.946×10^{-11}
	$SUS304$	0	201.04×10^{9}	3.079×10^{-4}	-6.534×10^{-7}	0
$\alpha(\frac{1}{k^0})$	Si_3N_4	0	5.8723×10^{-6}	9.095×10^{-4}	0	0
	$SUS304$	0	12.330×10^{-6}	8.086×10^{-4}	0	0
$\kappa(\frac{W}{mk^0})$	Si_3N_4	0	13.723	-1.032×10^{-3}	5.466×10^{-7}	-7.876×10^{-11}
	$SUS304$	0	15.379	-1.264×10^{-3}	2.092×10^{-6}	-7.223×10^{-10}
ϑ	Si_3N_4	0	0.2400	0	0	0
	$SUS304$	0	0.3262	-2.002×10^{-4}	3.797×10^{-7}	0

Table 2: Evaluation of frequency parameter for a square FG plate $(k=-0.81,\omega=\overline{\Omega}h\sqrt{\frac{\rho_c}{E_c}},\frac{l_a}{l_b}=1,\Delta T=0(C^0))$.

$\frac{l_a}{h}$	n	Present (FSDT)	[53] (FSDT)	[12] (HSDT)
•	0	0.2121	0.2121	0.2121
•	0.5	0.1814	0.1811	0.1819
5	1	0.1642	0.1636	0.164
•	4	0.1409	0.1401	0.1383
•	10	0.1331	0.1329	0.1306
•	0	0.0571	0.0577	0.0577
•	0.5	0.0485	0.0490	0.0491
10	1	0.0438	0.0442	0.0442
	4	0.0379	0.0383	0.0381
	10	0.0362	0.0366	0.0366

difference between the results is due to the solution theories, and the results of this study seem more accurate. Furthermore, the nonlinear frequency ratio is dependent on the amplitude of the vibration, and with increasing amplitude of the vibration; the effect of nonlinearity is increased.

In Fig. 2, the linear sound transmission loss of Al/Al_2O_3 rectangular FG plate extracted from the present study is compared with the results reported in [52] and CPT, showing good agreement.

In the above examples, the material properties are considered as temperature-independent and the thermal field is assumed to be a uniform temperature rise through the thickness. To ensure the correctness of the solution method, the nonlinear frequency ratio of free vibration extracted from this study has been compared with the results of [18]. Table 4 shows comparisons of nonlinear frequency ratio for $SUS304/Si_3N_4$ square plates with temperature-dependent material properties in the thermal ambiance. These comparisons show that the present results agree well with existing results.

In Fig. 3, the non-dimensional deflection of $SUS304/Si_3N_4$ square FG plate with temperature-dependent material properties in the thermal ambiance obtained by the

Table 3: Evaluation of the nonlinear frequency ratios for Al/Al_2O_3 square FG plate $(k=-0.81, \frac{l_a}{l_b}=40, \frac{l_a}{l_b}=1, \Delta T=0(C^0))$.

n	A	Present (FSDT)	[7] (FSDT)	[10] (HSDT)
•	0.25	1.0542	1.0529	1.0467
•	0.5	1.2005	1.1962	1.1758
0.2	0.75	1.4085	1.4005	1.3641
•	1	1.6553	1.6428	1.5911
•	1.5	2.2111	2.1895	2.1103
•	2	2.8091	2.7785	2.6755
•	0.25	1.0446	1.0473	1.0413
10	0.5	2.0468	2.0937	1.1563
•	0.75	1.3446	1.3630	1.3266
•	1	1.5581	1.5860	1.5335
•	1.5	2.0468	2.0937	2.0115
•	2	2.5785	2.6442	2.5355

HAM is compared to that obtained by the Runge-Kutta method shows excellent agreement.

Fig. 4 demonstrates the effects of aspect ratio $\frac{l_a}{l_b}$ on the nonlinear frequency ratio for different index of the power law values of $SUS304/Si_3N_4$ square FG plate with temperature-dependent material properties in the thermal ambiance. As in Figure 4 is seen for values $0<\frac{l_a}{l_b}<1$ by increasing the value of this geometrical ratio, the nonlinear

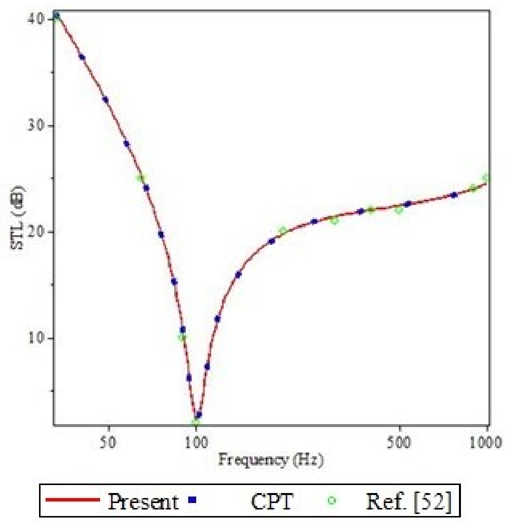

Figure 2: Comparison of the linear STL $(k=-0.81,\ l_a=0.38(m), l_b=0.15(m), h=0.00081(m),\ \Delta T=0(C^0),\ n=1000,\ \theta_i=60^0,\ \Phi_i=0^0)$.

Table 4: Comparison of nonlinear frequency ratios for $SUS304/Si_3N_4$ square plates in the thermal ambiance $(k=-0.35, T_t=400K, T_b=300K, l_a=0.2m, h=0.025m)$.

A		n			
		0	.05	1	2
0	Present (FSDT)	1	1	1	1
	Ref. [18] (HSDT)	1	1	1	1
0.2	Present (FSDT)	1.035	1.036	1.036	1.035
	Ref. [18] (HSDT)	1.022	1.022	1.022	1.022
0.4	Present (FSDT)	1.134	1.137	1.137	1.134
	Ref. [18] (HSDT)	1.084	1.084	1.084	1.082
0.6	Present (FSDT)	1.283	1.288	1.287	1.282
	Ref. [18] (HSDT)	1.181	1.181	1.180	1.176
0.8	Present (FSDT)	1.465	1.474	1.472	1.464
	Ref. [18] (HSDT)	1.303	1.302	1.301	1.299
1	Present (FSDT)	1.669	1.682	1.679	1.668
	Ref. [18] (HSDT)	1.446	1.444	1.442	1.668

frequency ratio is reduced and for values $1 < \frac{l_a}{l_b} < 4$ by increasing the $\frac{l_a}{l_b}$, the nonlinear frequency ratio is increased. At this point $\frac{l_a}{l_b} = 1$, which plate is square, the nonlinear frequency ratio is minimum. By distancing the plate from square geometry, the effect of nonlinear geometric terms of the problem is more intense. Also, by increasing the index values, nonlinear frequency ratio is decreased, and this is because the property of the graded material changes from ceramic to metal and the softening effect increases.

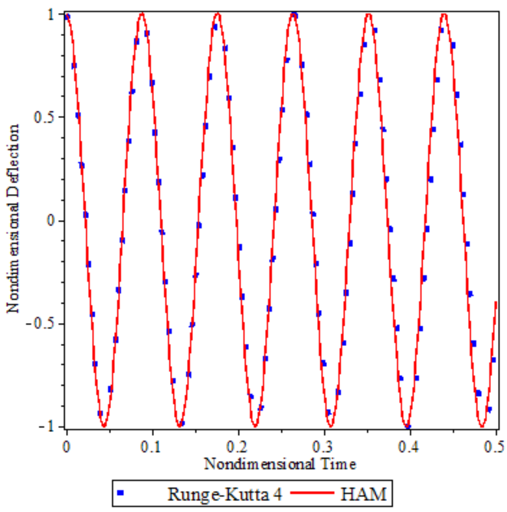

Figure 3: Comparison of the HAM results and those of Runge−Kutta method $(k=-0.35,\ T_t=400K, T_b=300K,$ $l_a=0.2m, h=0.025m,\ n=10, A=1, \theta_i=30^0, \Phi_i=30^0)$.

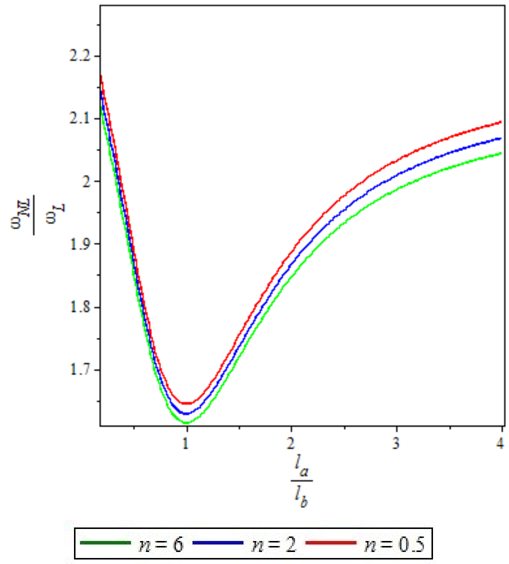

Figure 4: Changes in the nonlinear frequency ratios in terms of $\frac{l_a}{l_b}$ for different values of n ($k=-0.35$, $T_t=400K, T_b=300K, P_i=8.6(MP_a)$ $A=1, \theta_i=30^0$, $\Phi_i=30^0$).

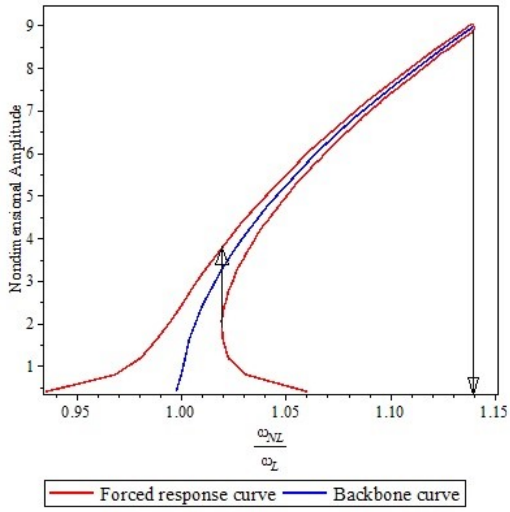

Figure 5: Backbone curve and hardening nonlinear forced response curve ($k=-0.81$, $a_0=0.25, a_1=25, a_2=-2.5\times10^{-4}, a_3=0.125$).

In Fig. 5, the blue curve signifies the free vibration behavior of the nonlinear system, presenting the dependency of the resonance on the vibration amplitude; this curve is so-called the backbone curve. The forced response is laid over on this curve to show that the backbone curve lies "in the middle" of the forced response curve; it is equidistant from

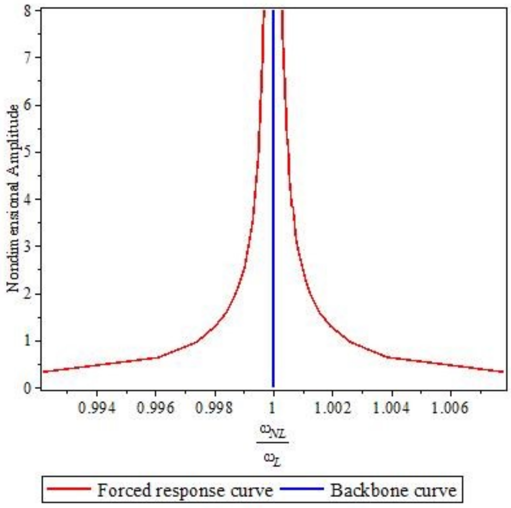

Figure 6: Backbone curve and linear forced response curve.

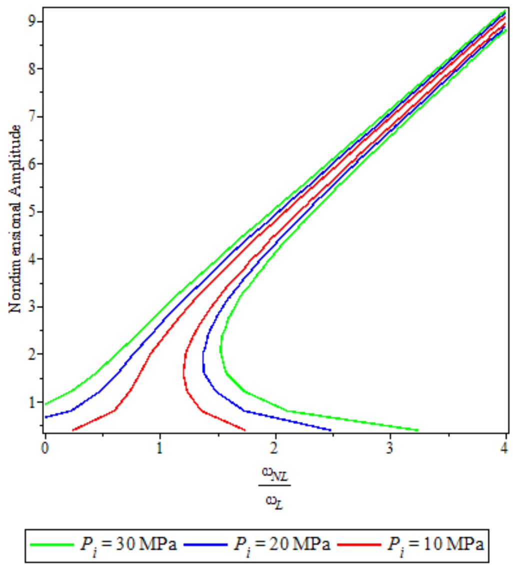

Figure 7: Influence of external acoustic pressure on the frequency-response $(k=-0.35,\ T_t=400K, T_b=300K, l_a=0.2m, h=0.025m, n=2,\ \theta_i=30^0,\ \Phi_i=30^0)$.

the forced response curve, where the distance is measured, as a first estimation, orthogonal to the backbone curve [60]. If the coefficient of the term has a positive power of 3 in the Doffing equation, it is called a hardening spring (tilts to the right). In hardening systems, the resonance frequency increases with increasing amplitude. Also, if the coefficient is negative, it is called a softening spring (tilts to the left). Resonance frequency

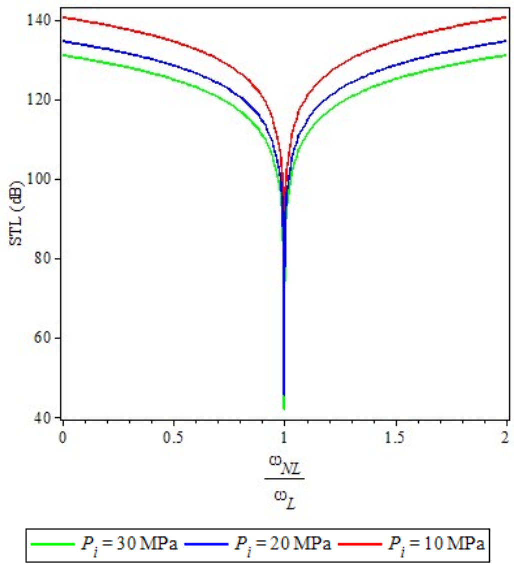

Figure 8: Effect of external acoustic pressure on the linear STL $(k=-0.35,\ T_t=400K, T_b=300K, l_a=0.2m, h=0.025m, n=2,\ \theta_i=30^0,\ \Phi_i=30^0)$.

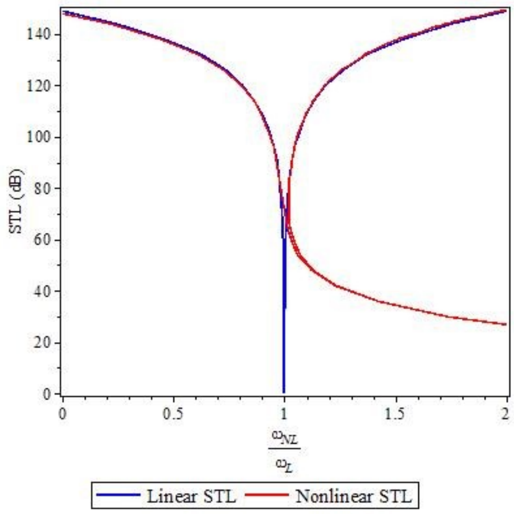

Figure 9: Comparison of the linear and nonlinear sound transmission loss.

declines with increasing amplitude for softening systems. The nonlinear response is not a single-valued function and a hysteretic effect occurs for increasing and decreasing excitation frequency. This gives rise to a jump phenomenon, indicated by arrows in Fig. 5.

Fig. 6 indicates the frequency-response of a Al/Al_2O_3 square FG plate to the natural frequency of the linear system. It is seen that the curve is not tilted to the right

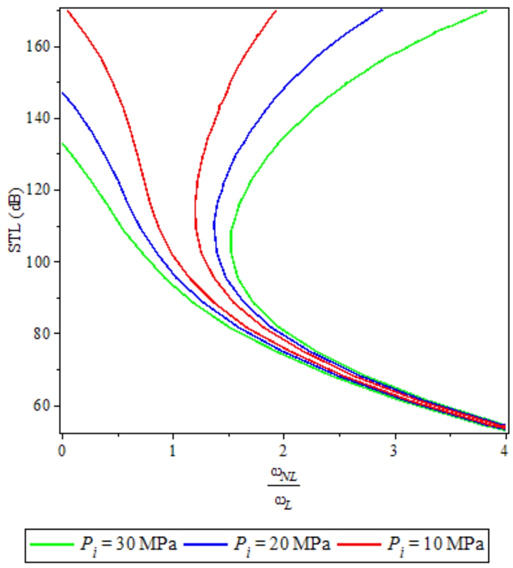

Figure 10: Influence of external acoustic pressure on the nonlinear STL $(k=-0.35,\ T_t=400K, T_b=300K, l_a=0.2m, h=0.025m, n=2,\ \theta_i=30^0,\ \Phi_i=30^0)$.

or left. An autonomous system is obtained if the external excitation is removed from the system. In a linear system, the frequency does not depend on the vibration amplitude. Fig. 7 illustrates the variations of non-dimensional amplitude against the nonlinear frequency ratio corresponding to different values of the external acoustic pressure in $SUS304/Si_3N_4$ square FG plate with temperature-dependent material properties in the thermal ambiance. It is perceived that increasing the external acoustic pressure leads to the distance from the forced response curve, and the hardening effects are decreased and also amplitude of vibration is found to be higher. This is because flexibility becomes higher. In Fig. 8, the variations of linear sound transmission loss versus nonlinear frequency ratio are exposed for different values of the external acoustic pressure in $SUS304/Si_3N_4$ square FG plate with temperature-dependent material properties in the thermal ambiance. It is seen that growing the external acoustic pressure leads to a reduction in sound transmission loss. This means that a lot of sounds are transmitted from the plate.

Fig. 9 compares linear sound transmission loss and nonlinear sound transmission loss versus nonlinear frequency ratio. As can be seen, the graph is tilted to the right, which indicates the hardening of the vibration system. Fig. 10 indicates the variations of nonlinear sound transmission loss versus nonlinear frequency ratio for various values of the external acoustic pressure in $SUS304/Si_3N_4$ square FG plate with temperature-dependent material properties in the thermal ambiance. It is seen that increasing the external acoustic pressure leads to a decrease in sound transmission loss. This means that a lot of sounds are transmitted from the plate, and this is because the hardening

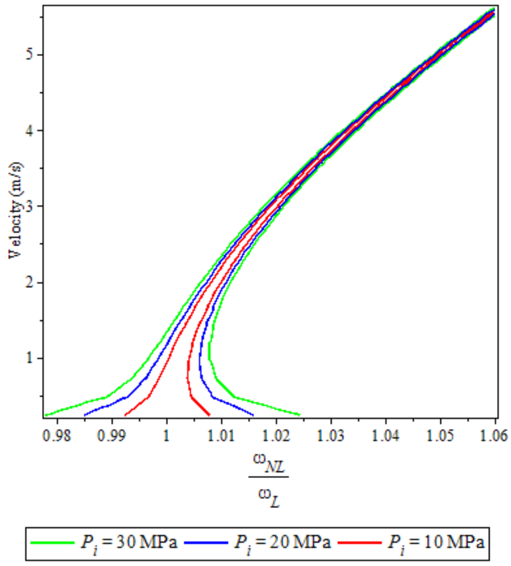

Figure 11: Effect of external acoustic pressure on the drive point velocity $(k=-0.35,\ T_t=400K, T_b=300K, l_a=0.2m, h=0.025m, n=2,\ \theta_i=30^0,\ \Phi_i=30^0)$.

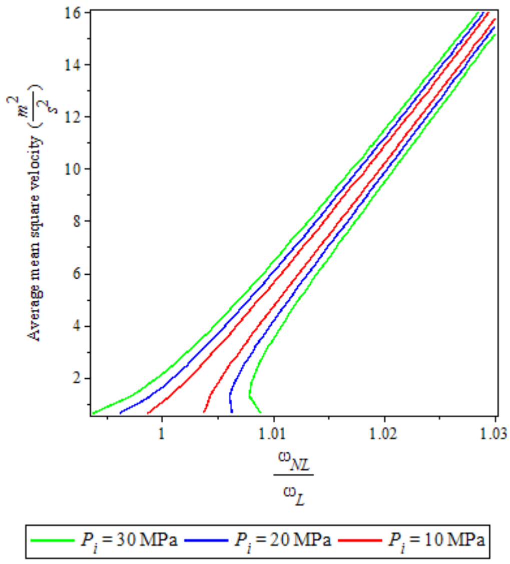

Figure 12: Influence of external acoustic pressure on the average mean square velocity $(k=-0.35,\ T_t=400K, T_b=300K, l_a=0.2m, h=0.025m, n=2,\ \theta_i=30^0,\ \Phi_i=30^0)$.

effect decreases. Figs. 11-13 illustrate the drive point velocity, the average means square velocity and the sound power level versus nonlinear frequency ratio for various values

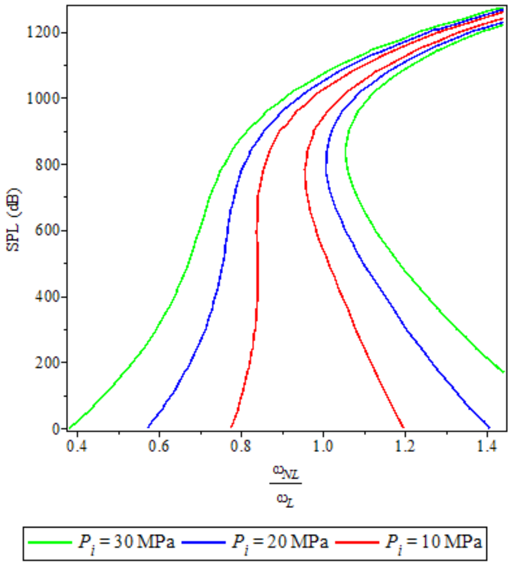

Figure 13: Sound power level due to point load excitation $(k=-0.35,\ T_t=400K, T_b=300K, l_a=0.2m, h=0.025m, n=2,\ \theta_i=30^0,\ \Phi_i=30^0)$.

of the external acoustic pressure in $SUS304/Si_3N_4$ square FG plate with temperature-dependent material properties in the thermal ambiance. It is seen that increasing the amplitude of the incident acoustic pressure leads to the distance from the response curve and the velocity, average means square velocity and the sound power level of the FG plate are increased.

Figs. 14-15 illustrate the variations of the frequency-response corresponding to different values of the incidence and azimuthal angles in $SUS304/Si_3N_4$ square FG plate with temperature-dependent material properties in the thermal ambiance. It is perceived that increasing the θ_i leads to the distance from the forced response curve, and also the hardening effects are increased. Also it is exhibits the increasing Φ_i does not have much effect on the frequency-response and this is due to the ignoring of external mean flow. Fig. 16 indicates the variations of the frequency-response for various values of the T_t and T_b in $SUS304/Si_3N_4$ square FG plate with temperature-dependent material properties in the thermal ambiance. It is seen that increasing the temperature changes lead to a decrease in hardening effects and is closer to the forced response curve. This is because the temperature changes have a softening effect on the total stiffness of the structure. This behavior is due to the fact that the natural frequencies decrease with increasing temperature changes.

Figs. 17-18 show the variations of nonlinear sound transmission loss versus nonlinear frequency ratio for various values of the θ_i and Φ_i in $SUS304/Si_3N_4$ square FG plate with temperature-dependent material properties in the thermal ambiance. It is seen that increasing the incident angle leads to an increase in sound transmission loss. This means that a bit of sound is transmitted from the plate. This is because that the sound waves

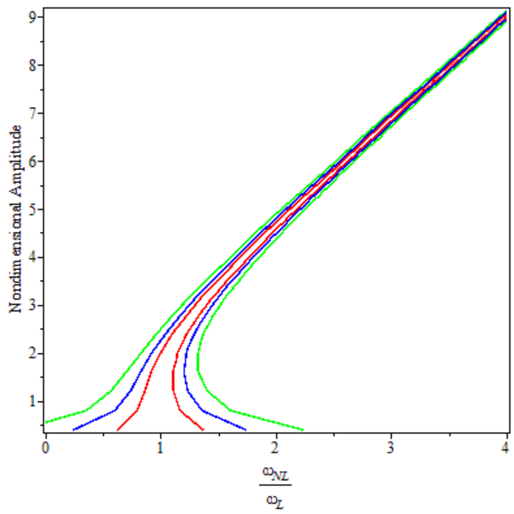

Figure 14: Influence of the incidence angle on the frequency-response $(k=-0.35,\ T_t=400K, T_b=300K, l_a=0.2m, h=0.025m, n=2,\ \theta_i=30^0,\ \Phi_i=30^0)$.

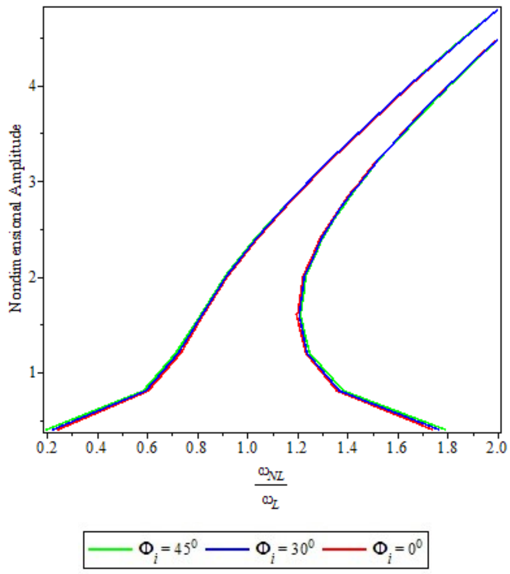

Figure 15: Effect of the azimuthal angle on the frequency-response $(k=-0.35,\ T_t=400K, T_b=300K, l_a=0.2m, h=0.025m, n=2,\ \theta_i=30^0,\ \Phi_i=30^0)$.

with larger incident angles pass through the structure less than sound waves with smaller incident angles. Also it is observed that increasing Φ_i does not have much effect on the STL value, and this is due to the ignoring of external mean flow. Fig. 19 exhibits the variations of nonlinear sound transmission loss versus nonlinear frequency ratio for various

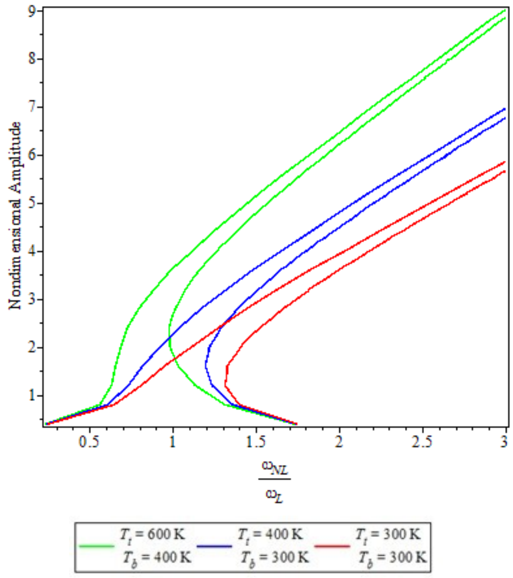

Figure 16: Influence of the temperature changes on the frequency-response ($k=-0.35$, $l_a=0.2m, h=0.025m, n=2$, $\theta_i=30^0$, $\Phi_i=30^0$).

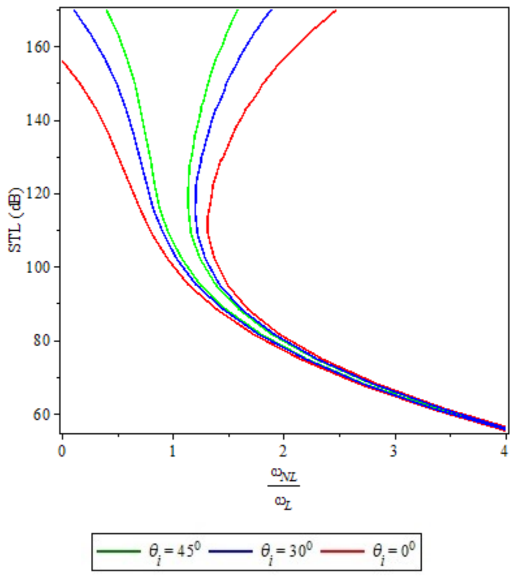

Figure 17: Effect of the incidence angle on the nonlinear STL ($k=-0.35$, $T_t=400K, T_b=300K, l_a=0.2m, h=0.025m, n=2$, $\Phi_i=30^0$).

values of the T_t and T_b in $SUS304/Si_3N_4$ square FG plate with temperature-dependent material properties in the thermal ambiance. It is seen that increasing the temperature

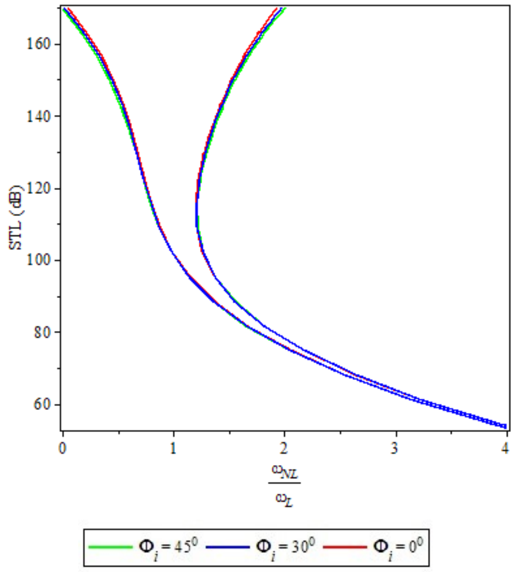

Figure 18: Influence of the azimuthal angle on the nonlinear STL $(k=-0.35,\ T_t=400K, T_b=300K, l_a=0.2m, h=0.025m, n=2,\ \Phi_i=30^0)$.

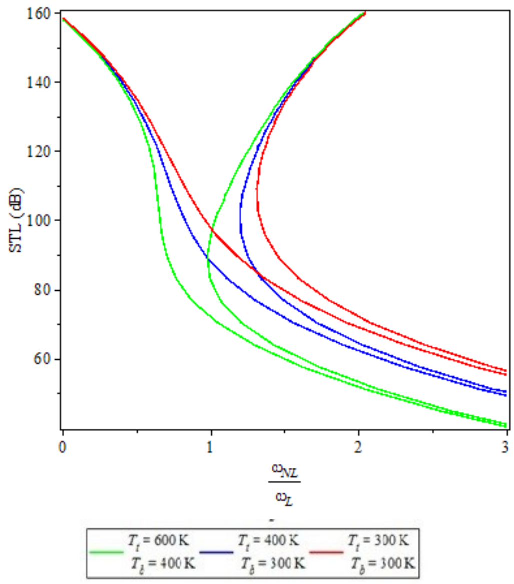

Figure 19: Effect of the temperature changes on the nonlinear STL $(k=-0.35,\ T_t=400K, T_b=300K, l_a=0.2m, h=0.025m, n=2,\ \theta_i=30^0)$.

changes lead to a decrease in sound transmission loss. This means that a lot of sounds are transmitted from the plate. This is because that the temperature changes have a soft-

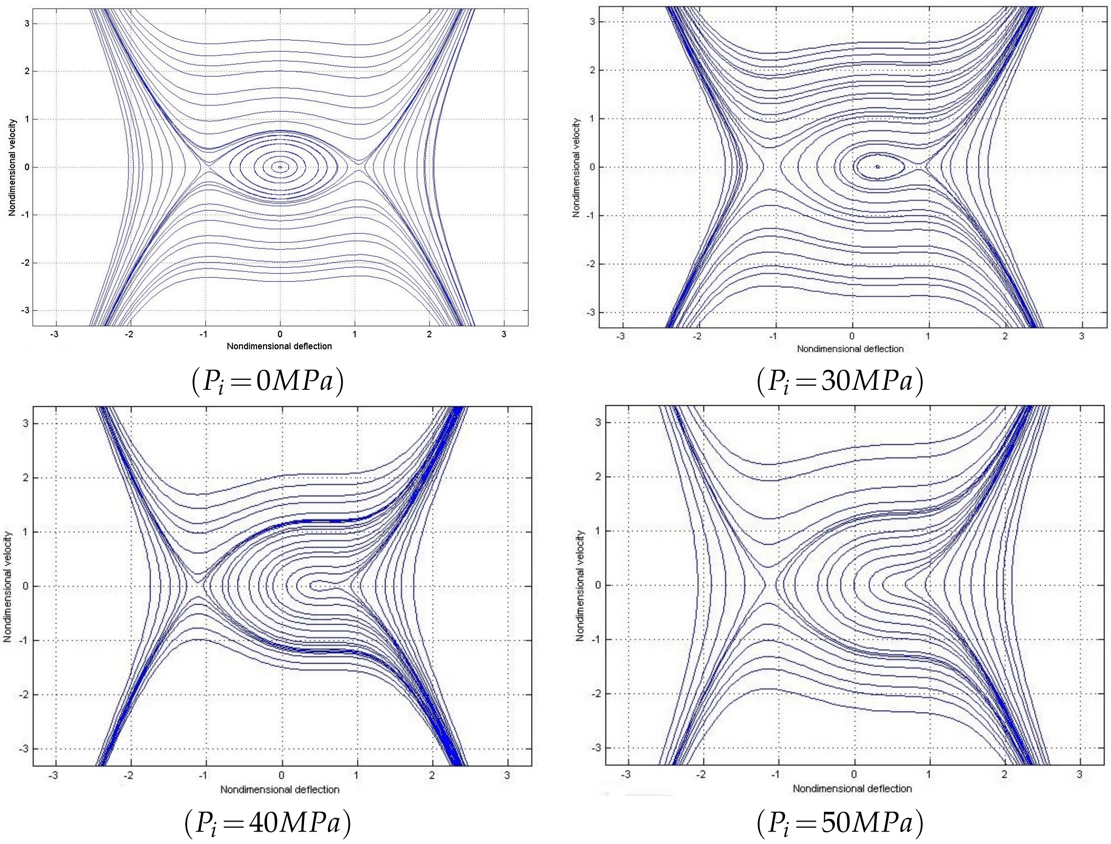

Figure 20: Phase diagram of the FG plate with external acoustic pressure ($k = -0.81$, $\frac{l_a}{l_b} = 5$, $\frac{l_a}{h} = 20$,$\Delta T = 20(C^0)$,$n = 2$, $\theta_i = 30^0$,$\Phi_i = 30^0$).

ening effect on the total stiffness of the structure.

In Fig. 20, the instability and its behavior are shown with the help of the phase diagram (the non-dimensional velocity $\left(\frac{dW}{dT}\right)$ versus non-dimensional deflection) for the FG plate with temperature-independent material properties in the thermal ambiance. It can be concluded that by inputting external acoustic pressure, the stable region decreases until instability occurs. In this case study, temperature change across the thickness of the plate is assumed uniform temperature rise.

6 Conclusions

In this paper, the nonlinear vibroacoustic behavior of a rectangular plate made of functionally graded material that is exposed to an incident oblique plane sound wave and thermal loads is determined by using the first-order shear deformation theory. The

Galerkin method has been utilized for reducing the governing nonlinear partial differential equations to nonlinear ordinary differential ones in the time domain. The homotopy analysis method has been used for solving the resulting nonlinear ordinary differential equation of motion. The results display that the jump phenomenon can be seen in the frequency response of plate vibration. The most important observations are summarized as follows:

1. By increasing the aspect ratio of the functionally graded plate, the nonlinear frequency ratio reduces for values $0<\frac{l_a}{l_b}<1$ and increases for values $1<\frac{l_a}{l_b}<4$. Also, by increasing the index of the power law values of the functionally graded plate, the nonlinear frequency ratio is decreased.

2. The nonlinear response is not a single-valued function and a hysteretic effect occurs for increasing and decreasing excitation frequency of the functionally graded plate. This causes a jump phenomenon.

3. Increasing the external acoustic pressure leads to the distance from the forced response curve, reducing the hardening effects and increasing the vibration amplitude of the functionally graded plate and by increasing the amplitude of the vibration, the effect of nonlinearity is increased.

4. Growing in external acoustic pressure reduced the sound transmission losses due to reduced hardening effects transmitted from the functionally graded plate.

5. An increase in the amplitude of the incident sound pressure leads to increase in the velocity, the mean square velocity and the sound power level of the functionally graded plate.

6. Increasing the incidence angle leads to increase in hardening effects and sound transmission loss of the functionally graded plate.

7. Growing the azimuthal angle does not have much effect on the frequency-response and sound transmission loss of the functionally graded plate in the absence of the external mean flow.

8. Increasing temperature changes lead to decrease in hardening effects and sound transmission loss of the functionally graded plate.

9. By inputting external acoustic pressure, the stable region decreases until instability occurs.

Appendix A. Amplitudes of the reflected and transmitted waves

$$
\begin{aligned}
P_r = &\frac{1}{4}\left(\left(-\pi^6 m^3 n^3 \rho + \pi^4 m^3 n \rho k_y^2 l_b^2 + \pi^4 m n^3 \rho k_x^2 l_a^2 - \pi^2 m n \rho k_x^2 k_y^2 l_a^2 l_b^2\right)\left(\frac{d^2}{dt^2} W_{mn}(t)\right)\right), \\
&\cdot\left(n\pi^2 k_z m\left(-Im\pi^2 n(-1)^m(-1)^n e^{I(\Omega t - k_x l_a - k_y l_b)},\right.\right. \\
&\left.\left.+Im\pi^2 n(-1)^m e^{I(\Omega t - k_x l_a)} + Im\pi^2 n(-1)^n e^{I(\Omega t - k_y l_b)} - I\pi^2 e^{I\Omega t} mn\right)\right)^{-1} \\
&+\frac{1}{4}\left(\left(-4I\pi^4 e^{I\Omega t} m^2 k_z n^2 - 4Im^2\pi^4 n^2 k_z(-1)^m(-1)^n e^{I(\Omega t - k_x l_a - k_y l_b)},\right.\right. \\
&\left.\left.+4Im^2\pi^4 n^2 k_z(-1)^n e^{I(\Omega t - k_y l_b)} + 4Im^2\pi^4 n^2 k_z(-1)^m e^{I(\Omega t - k_x l_a)}\right)P_i\right), \\
&\cdot\left(n\pi^2 k_z m\left(-Im\pi^2 n(-1)^m(-1)^n e^{I(\Omega t - k_x l_a - k_y l_b)} + Im\pi^2 n(-1)^m e^{I(\Omega t - k_x l_a)}\right.\right. \\
&\left.\left.+Im\pi^2 n(-1)^n e^{I(\Omega t - k_y l_b)} - I\pi^2 e^{I\Omega t} mn\right)\right)^{-1}, \\
P_t = &-\frac{1}{4}\left(\rho\left(\frac{d^2}{dt^2} W_{mn}(t)\right)\left(-\pi^6 m^3 n^3 + \pi^4 m^3 n k_y^2 l_b^2 + \pi^4 m n^3 k_x^2 l_a^2 - \pi^2 m n k_x^2 k_y^2 l_a^2 l_b^2\right)\right) \\
&\cdot\left(n\pi^2 k_z m\left(-Im\pi^2 n(-1)^m(-1)^n e^{I(\Omega t - k_x l_a - k_y l_b)} + Im\pi^2 n(-1)^m e^{I(\Omega t - k_x l_a)}\right.\right. \\
&\left.\left.+Im\pi^2 n(-1)^n e^{I(\Omega t - k_y l_b)} - I\pi^2 e^{I\Omega t} mn\right)\right)^{-1}.
\end{aligned}
$$

Appendix B. Coefficients of Eqs.(2.18)-(2.20)

$$
\begin{aligned}
&\Pi_{11} = \frac{4}{9}\frac{(1-(-1)^m)(1-(-1)^n)}{mn\pi^2}\left(\frac{(A_{12}-A_{66})m\pi^3 n^2}{l_b^2 l_a} - \frac{2A_{11}m^3\pi^3}{l_a^3}\right), \\
&\Pi_{12} = \frac{A_{11}m^2\pi^2}{l_a^2} + \frac{A_{66}m^2\pi^2}{l_b^2}, \quad \Pi_{13} = \frac{m\pi^2 n(A_{12}+A_{66})}{l_a l_b}, \quad \Pi_{14} = \frac{B_{11}m^2\pi^2}{l_a^2} + \frac{B_{66}n^2\pi^2}{l_b^2},
\end{aligned}
$$

$$\Pi_{15}=\frac{m\pi^2 n(B_{12}+B_{66})}{l_a l_b},$$

$$\Pi_{21}=\frac{4}{9}\frac{(1-(-1)^m)(1-(-1)^n)}{mn\pi^2}\Big(\frac{(A_{12}-A_{66})m^2\pi^3 n}{l_a^2 l_b}-\frac{2A_{22}n^3\pi^3}{l_b^3}\Big),$$

$$\Pi_{22}=\Pi_{13},\quad \Pi_{23}=\frac{A_{66}m^2\pi^2}{l_a^2}+\frac{A_{22}n^2\pi^2}{l_b^2},\quad \Pi_{24}=\frac{m\pi^2 n(B_{12}+B_{66})}{l_a l_b},$$

$$\Pi_{25}=\frac{B_{66}m^2\pi^2}{l_a^2}+\frac{B_{22}n^2\pi^2}{l_b^2},\quad \Pi_{31}=\frac{9}{32}\frac{A_{11}m^4\pi^4}{l_a^4}+\frac{9}{32}\frac{A_{22}n^4\pi^4}{l_b^4}+\frac{1}{16}\frac{n^2\pi^4 m^2(A_{12}+2A_{66})}{l_b^2 l_a^2},$$

$$\Pi_{32}=K\left(\frac{A_{55}m^2\pi^2}{l_a^2}+\frac{A_{44}n^2\pi^2}{l_b^2}\right),\quad \Pi_{33}=\frac{KA_{55}m\pi}{l_a},\quad \Pi_{34}=\frac{KA_{44}n\pi}{l_b},$$

$$\Pi_{35}=\frac{8}{9}\frac{(1-(-1)^m)(1-(-1)^n)}{mn\pi^2}\left(\frac{(A_{12}-A_{66})m\pi^3 n^2}{l_b^2 l_a}+\frac{A_{11}m^3\pi^3}{l_a^3}\right),$$

$$\Pi_{36}=\frac{8}{9}\frac{(1-(-1)^m)(1-(-1)^n)}{mn\pi^2}\left(\frac{(A_{12}-A_{66})m^2\pi^3 n}{l_a^2 l_b}+\frac{A_{22}n^3\pi^3}{l_b^3}\right),$$

$$\Pi_{37}=\frac{8}{9}\frac{(1-(-1)^m)(1-(-1)^n)}{mn\pi^2}\left(\frac{(B_{12}-B_{66})m\pi^3 n^2}{l_b^2 l_a}+\frac{B_{11}m^3\pi^3}{l_a^3}\right),$$

$$\Pi_{38}=\frac{8}{9}\frac{(1-(-1)^m)(1-(-1)^n)}{mn\pi^2}\left(\frac{(B_{12}-B_{66})m^2\pi^3 n}{l_b^2 l_a}+\frac{B_{22}n^3\pi^3}{l_b^3}\right),$$

$$\Pi_{39}=\frac{8\pi^2 P_i H_0}{(k_x^2 k_y^2 l_a^2 l_b^2-\pi^2 k_x^2 l_a^2-\pi^2 k_y^2 l_b^2+\pi^4)I_0},$$

$$\Pi_{41}=\frac{4}{9}\frac{(1-(-1)^m)(1-(-1)^n)}{mn\pi^2}\left(\frac{(B_{12}-B_{66})m\pi^3 n^2}{l_b^2 l_a}-\frac{2B_{11}m^3\pi^3}{l_a^3}\right),$$

$$\Pi_{42}=\Pi_{33},\quad \Pi_{43}=\Pi_{14},\quad \Pi_{44}=\Pi_{15},$$

$$\Pi_{45}=\frac{D_{11}m^2\pi^2}{l_a^2}+\frac{D_{66}n^2\pi^2}{l_b^2}+KA_{55},\quad \Pi_{46}=\frac{m\pi^2 n(D_{12}+D_{66})}{l_a l_b},$$

$$\Pi_{41}=\frac{4}{9}\frac{(1-(-1)^m)(1-(-1)^n)}{mn\pi^2}\left(\frac{(B_{12}-B_{66})m^2\pi^3 n}{l_a^2 l_b}-\frac{2B_{22}n^3\pi^3}{l_b^3}\right),$$

$$\Pi_{52}=\Pi_{34},\quad \Pi_{53}=\Pi_{15},\quad \Pi_{54}=\Pi_{25},\quad \Pi_{55}=\Pi_{46},$$

$$\Pi_{56}=\frac{D_{66}m^2\pi^2}{l_a^2}+\frac{D_{22}n^2\pi^2}{l_b^2}+KA_{44},$$

$$
\begin{aligned}
G=&\Pi_{15}\Pi_{24}\Pi_{44}\Pi_{53}-\Pi_{14}\Pi_{25}\Pi_{44}\Pi_{53}-\Pi_{15}\Pi_{23}\Pi_{45}\Pi_{53}+\Pi_{13}\Pi_{25}\Pi_{45}\Pi_{53}\\
&+\Pi_{14}\Pi_{23}\Pi_{46}\Pi_{53}-\Pi_{13}\Pi_{24}\Pi_{46}\Pi_{53}-\Pi_{15}\Pi_{24}\Pi_{43}\Pi_{54}+\Pi_{14}\Pi_{25}\Pi_{43}\Pi_{54}\\
&+\Pi_{15}\Pi_{22}\Pi_{45}\Pi_{54}-\Pi_{12}\Pi_{25}\Pi_{45}\Pi_{54}-\Pi_{14}\Pi_{22}\Pi_{46}\Pi_{54}+\Pi_{12}\Pi_{24}\Pi_{46}\Pi_{54}\\
&+\Pi_{15}\Pi_{23}\Pi_{43}\Pi_{55}-\Pi_{13}\Pi_{25}\Pi_{43}\Pi_{55}-\Pi_{15}\Pi_{22}\Pi_{44}\Pi_{55}+\Pi_{12}\Pi_{25}\Pi_{44}\Pi_{55}\\
&+\Pi_{13}\Pi_{22}\Pi_{46}\Pi_{55}-\Pi_{12}\Pi_{23}\Pi_{46}\Pi_{55}-\Pi_{14}\Pi_{23}\Pi_{43}\Pi_{56}+\Pi_{13}\Pi_{24}\Pi_{43}\Pi_{56}\\
&+\Pi_{14}\Pi_{22}\Pi_{44}\Pi_{56}-\Pi_{12}\Pi_{24}\Pi_{44}\Pi_{56}-\Pi_{13}\Pi_{22}\Pi_{45}\Pi_{56}+\Pi_{12}\Pi_{23}\Pi_{45}\Pi_{56},\\
T_{11}=&\frac{1}{G}(\Pi_{23}\Pi_{45}\Pi_{56}-\Pi_{23}\Pi_{46}\Pi_{55}-\Pi_{24}\Pi_{44}\Pi_{54}+\Pi_{24}\Pi_{46}\Pi_{54}+\Pi_{25}\Pi_{44}\Pi_{55}\\
&-\Pi_{25}\Pi_{45}\Pi_{54}),\\
T_{12}=&\frac{1}{G}(-\Pi_{13}\Pi_{45}\Pi_{56}+\Pi_{13}\Pi_{46}\Pi_{55}+\Pi_{14}\Pi_{44}\Pi_{56}-\Pi_{14}\Pi_{46}\Pi_{54}-\Pi_{15}\Pi_{44}\Pi_{55}\\
&+\Pi_{15}\Pi_{45}\Pi_{54}),\\
T_{13}=&\frac{1}{G}(\Pi_{13}\Pi_{24}\Pi_{56}-\Pi_{13}\Pi_{25}\Pi_{55}-\Pi_{14}\Pi_{23}\Pi_{56}+\Pi_{14}\Pi_{25}\Pi_{54}+\Pi_{15}\Pi_{23}\Pi_{55}\\
&-\Pi_{15}\Pi_{24}\Pi_{54}),\\
T_{14}=&\frac{1}{G}(-\Pi_{13}\Pi_{24}\Pi_{46}+\Pi_{13}\Pi_{25}\Pi_{45}+\Pi_{14}\Pi_{23}\Pi_{46}-\Pi_{14}\Pi_{25}\Pi_{44}-\Pi_{15}\Pi_{23}\Pi_{45}\\
&+\Pi_{15}\Pi_{24}\Pi_{44}),\\
T_{21}=&\frac{1}{G}(-\Pi_{22}\Pi_{45}\Pi_{56}+\Pi_{22}\Pi_{46}\Pi_{55}+\Pi_{24}\Pi_{43}\Pi_{56}-\Pi_{24}\Pi_{46}\Pi_{53}-\Pi_{25}\Pi_{43}\Pi_{55}\\
&+\Pi_{25}\Pi_{45}\Pi_{53}),\\
T_{22}=&\frac{1}{G}(\Pi_{12}\Pi_{45}\Pi_{56}-\Pi_{12}\Pi_{46}\Pi_{55}-\Pi_{14}\Pi_{43}\Pi_{56}+\Pi_{14}\Pi_{46}\Pi_{53}+\Pi_{15}\Pi_{43}\Pi_{55}\\
&-\Pi_{15}\Pi_{45}\Pi_{53}),\\
T_{23}=&\frac{1}{G}(-\Pi_{12}\Pi_{24}\Pi_{56}+\Pi_{12}\Pi_{25}\Pi_{55}+\Pi_{14}\Pi_{22}\Pi_{56}-\Pi_{14}\Pi_{25}\Pi_{53}-\Pi_{15}\Pi_{22}\Pi_{55}\\
&+\Pi_{15}\Pi_{24}\Pi_{53}),\\
T_{24}=&\frac{1}{G}(\Pi_{12}\Pi_{24}\Pi_{46}-\Pi_{12}\Pi_{25}\Pi_{45}-\Pi_{14}\Pi_{22}\Pi_{46}+\Pi_{14}\Pi_{25}\Pi_{43}+\Pi_{15}\Pi_{22}\Pi_{45}\\
&-\Pi_{15}\Pi_{24}\Pi_{43}),\\
T_{31}=&\frac{1}{G}(\Pi_{22}\Pi_{44}\Pi_{56}-\Pi_{22}\Pi_{46}\Pi_{54}-\Pi_{23}\Pi_{43}\Pi_{56}+\Pi_{23}\Pi_{46}\Pi_{53}+\Pi_{25}\Pi_{43}\Pi_{54}\\
&-\Pi_{25}\Pi_{44}\Pi_{53}),\\
T_{32}=&\frac{1}{G}(-\Pi_{12}\Pi_{44}\Pi_{56}+\Pi_{12}\Pi_{46}\Pi_{54}+\Pi_{13}\Pi_{43}\Pi_{56}-\Pi_{13}\Pi_{46}\Pi_{53}-\Pi_{15}\Pi_{43}\Pi_{54}\\
&+\Pi_{15}\Pi_{44}\Pi_{53}),\\
T_{33}=&\frac{1}{G}(\Pi_{12}\Pi_{23}\Pi_{56}-\Pi_{12}\Pi_{25}\Pi_{54}-\Pi_{13}\Pi_{22}\Pi_{56}+\Pi_{13}\Pi_{25}\Pi_{53}+\Pi_{15}\Pi_{22}\Pi_{54}\\
&-\Pi_{15}\Pi_{23}\Pi_{53}),
\end{aligned}
$$

$$
\begin{aligned}
T_{34}=&\frac{1}{G}(-\Pi_{12}\Pi_{23}\Pi_{46}+\Pi_{12}\Pi_{25}\Pi_{44}+\Pi_{13}\Pi_{22}\Pi_{46}-\Pi_{13}\Pi_{25}\Pi_{43}-\Pi_{15}\Pi_{22}\Pi_{44}\\
&\qquad+\Pi_{15}\Pi_{23}\Pi_{43}),\\
T_{41}=&\frac{1}{G}(-\Pi_{22}\Pi_{44}\Pi_{55}+\Pi_{22}\Pi_{45}\Pi_{54}+\Pi_{23}\Pi_{43}\Pi_{55}-\Pi_{23}\Pi_{45}\Pi_{53}-\Pi_{24}\Pi_{43}\Pi_{54}\\
&\qquad+\Pi_{24}\Pi_{44}\Pi_{53}),\\
T_{42}=&\frac{1}{G}(\Pi_{12}\Pi_{44}\Pi_{55}-\Pi_{12}\Pi_{45}\Pi_{54}-\Pi_{13}\Pi_{43}\Pi_{55}+\Pi_{13}\Pi_{45}\Pi_{53}+\Pi_{14}\Pi_{43}\Pi_{54}\\
&\qquad-\Pi_{14}\Pi_{44}\Pi_{53}),\\
T_{43}=&\frac{1}{G}(-\Pi_{12}\Pi_{23}\Pi_{55}+\Pi_{12}\Pi_{24}\Pi_{54}+\Pi_{13}\Pi_{22}\Pi_{55}-\Pi_{13}\Pi_{24}\Pi_{53}-\Pi_{14}\Pi_{22}\Pi_{54}\\
&\qquad+\Pi_{14}\Pi_{23}\Pi_{53}),\\
T_{44}=&\frac{1}{G}(\Pi_{12}\Pi_{23}\Pi_{45}-\Pi_{12}\Pi_{24}\Pi_{44}-\Pi_{13}\Pi_{22}\Pi_{45}+\Pi_{13}\Pi_{24}\Pi_{43}+\Pi_{14}\Pi_{22}\Pi_{44}\\
&\qquad-\Pi_{14}\Pi_{23}\Pi_{43}),\\
H_0=&\sqrt{H_1^2+H_2^2},\quad \Phi=\frac{H_2}{H_1},\\
H_2=&\sin(\Omega t-k_xl_a)+\sin(\Omega t-k_yl_b)+\sin(\Omega t-k_xl_a-k_yl_b)+\sin(\Omega t),\\
H_1=&\cos(\Omega t-k_xl_a)+\cos(\Omega t-k_yl_b)+\cos(\Omega t-k_xl_a-k_yl_b)+\cos(\Omega t).
\end{aligned}
$$

Appendix C. Coefficients of Eq. (2.30)

$$
\begin{aligned}
a_0=&-\frac{8\sqrt{\frac{\rho_m}{E_m}}\pi^2P_iH_0}{I_0(k_x^2k_y^2l_a^2l_b^2-\pi^2k_x^2l_a^2-\pi^2k_y^2l_b^2+\pi^4)},\\
a_1=&\frac{1}{I_0}\left(h\sqrt{\frac{\rho_m}{E_m}}(-1\cdot\Pi_{33}\Pi_{42}T_{33}-1\cdot\Pi_{33}\Pi_{52}T_{34}-1\cdot\Pi_{34}\Pi_{42}T_{43}-1\cdot\Pi_{34}\Pi_{52}T_{44}+\Pi_{32})\right),\\
a_2=&\frac{1}{I_0}\left(h^2\sqrt{\frac{\rho_m}{E_m}}(\Pi_{35}\Pi_{42}T_{13}+\Pi_{35}\Pi_{52}T_{14}+\Pi_{36}\Pi_{42}T_{23}+\Pi_{36}\Pi_{52}T_{24},\right.\\
&\quad+\Pi_{11}\Pi_{33}T_{31}+\Pi_{21}\Pi_{33}T_{32}+\Pi_{33}\Pi_{41}T_{33}+\Pi_{37}\Pi_{42}T_{33}+\Pi_{33}\Pi_{51}T_{34},\\
&\quad+\Pi_{37}\Pi_{52}T_{34}+\Pi_{11}\Pi_{34}T_{41}+\Pi_{21}\Pi_{34}T_{42}+\Pi_{34}\Pi_{41}T_{43}+\Pi_{38}\Pi_{42}T_{43}\\
&\quad\left.+\Pi_{34}\Pi_{51}T_{44}+\Pi_{38}\Pi_{52}T_{44})\right),
\end{aligned}
$$

$$a_3 = \frac{1}{I_0}\left(h^3\sqrt{\frac{\rho_m}{E_m}}(\Pi_{31} - 1\cdot\Pi_{21}\Pi_{35}T_{12} - 1\cdot\Pi_{35}\Pi_{41}T_{13} - 1\cdot\Pi_{35}\Pi_{51}T_{14} \right.$$
$$- 1\cdot\Pi_{11}\Pi_{36}T_{21} - 1\cdot\Pi_{21}\Pi_{36}T_{22} - 1\cdot\Pi_{36}\Pi_{41}T_{23} - 1\cdot\Pi_{36}\Pi_{51}T_{24}$$
$$- 1\cdot\Pi_{11}\Pi_{37}T_{31} - 1\cdot\Pi_{21}\Pi_{37}T_{32} - 1\cdot\Pi_{37}\Pi_{41}T_{33} - 1\cdot\Pi_{37}\Pi_{51}T_{34}$$
$$\left. - 1\cdot\Pi_{11}\Pi_{38}T_{41} - 1\cdot\Pi_{21}\Pi_{38}T_{42} - 1\cdot\Pi_{38}\Pi_{41}T_{43} - 1\cdot\Pi_{38}\Pi_{51}T_{44} - 1\cdot\Pi_{11}\Pi_{35}T_{11})\right).$$

References

[1] L. E. KINSLER, A. R. FREY, A. B. COPPENS AND J. V. SANDERS, Fundamentals of Acoustics, John Wiley & Sons, 2000.

[2] D. D. REYNOLDS, Engineering Principles of Acoustics: Noise and Vibration Control, Allyn and Bacon, 1981.

[3] L. CREMER AND M. HECKL, Structure-Borne Sound: Structural Vibrations and Sound Radiation at Audio Frequencies, Springer Science & Business Media, 2013.

[4] M. P. NORTON AND D. G. KARCZUB, Fundamentals of Noise and Vibration Analysis for Engineers, Cambridge University Press, 2003.

[5] P. JEYARAJ, N. GANESAN AND C. PADMANABHAN, *Vibration and acoustic response of a composite plate with inherent material damping in a thermal environment,* Journal of Sound and Vibration, 320(1-2) (2009), pp. 322–338.

[6] Y. GHOLAMI AND R. A. KHALKHALI, *Numerical analysis of nonlinear forced vibration of functionally graded rectangular plates with various boundary conditions using 3D theory of elasticity,* Journal of Mechanical Engineering, 2019. 49(2) (2019), p. 87.

[7] S. HASHEMI AND A. ASGHAR JAFARI, *Nonlinear free vibration analysis of functionally graded rectangular plate using modified Lindstedt-Poincare method, In Persian,* Journal of Science and Technology of Composites, 6 (2020), pp. 637–648.

[8] H.-T. THAI AND D.-H. CHOI, *A simple first-order shear deformation theory for the bending and free vibration analysis of functionally graded plates,* Composite Structures, 101 (2013), pp. 332–340.

[9] S. J. SINGH AND S. P. HARSHA, *Static analysis of functionally graded plate using nonlinear classical plate theory with von Karman strains: a complex solution analysis,* Advances in Engineering Design, Springer, (2019), pp. 1–20.

[10] A. A. YAZDI, *Homotopy perturbation method for nonlinear vibration analysis of functionally graded plate,* Journal of Vibration and Acoustics, 135(2) (2013).

[11] J. YANG AND H.-S. SHEN, *Vibration characteristics and transient response of shear-deformable functionally graded plates in thermal environments,* Journal of Sound and vibration, 255(3) (2022), pp. 579–602.

[12] H. MATSUNAGA, *Free vibration and stability of functionally graded plates according to a 2-D higher-order deformation theory,* Composite structures, 82(4) (2000), pp. 499–512.

[13] S. S. VEL AND R. BATRA, *Three-dimensional exact solution for the vibration of functionally graded rectangular plates,* Journal of Sound and Vibration, 272(3-5) (2004), pp. 703–730.

[14] Y. HAO, W. ZHANG AND J. YANG, *Nonlinear oscillation of a cantilever FGM rectangular plate based on third-order plate theory and asymptotic perturbation method,* Composites Part B: Engineering, 42(3) (2011), pp. 402–413.

[15] W. ZHANG, Y. HAO, X. GUO AND L. CHEN, *Complicated nonlinear responses of a simply supported FGM rectangular plate under combined parametric and external excitations,* Meccanica, 47(4) (2012), pp. 985–1014.

[16] V. DOGAN, *Nonlinear vibration of FGM plates under random excitation,* Composite Structures, 95 (2013), p. 366–374.

[17] X.-L. HUANG, AND H.-S. SHEN, *Nonlinear vibration and dynamic response of functionally graded plates in thermal environments,* International Journal of Solids and Structures, 41(9-10) (2004), pp. 2403–2427.

[18] H.-S. SHEN, Functionally Graded Materials: Nonlinear Analysis of Plates and Shells, CRC press, 2016.

[19] F. SAMADANI, P. MORADWEYSI, K. HOSSEINI AND A. DARVIZEH, *Application of homotopy analysis method for the pull-in and nonlinear vibration analysis of nanobeams using a nonlocal Euler–Bernoulli beam model,* Zeitschrift für Naturforschung, 72(12) (2017), pp. 1093–1104.

[20] S. LIAO, Homotopy Analysis Method in Nonlinear Differential Equations, Springer, 2012.

[21] J. TORABI, R.ANSARI, A. ZABIHI AND K. HOSSEINI, *Dynamic and pull-in instability analyses of functionally graded nanoplates via nonlocal strain gradient theory,* Mechanics Based Design of Structures and Machines, (2020), pp. 1–21

[22] A. YOOSEFIAN, M. GOLMAKANI AND M. SADEGHIAN, *Nonlinear bending of functionally graded sandwich plates under mechanical and thermal load,* Communications in Nonlinear Science and Numerical Simulation, 84 (2020), p. 105161.

[23] H. AMIRINEZHAD, A. TARKASHVAND AND R. TALEBITOOTITOOTI, *Acoustic wave transmission through a polymeric foam plate using the mathematical model of functionally graded viscoelastic (FGV) material,* Thin-Walled Structures, 148 (2020), p. 106466.

[24] S. LI AND X. LI, *The effects of distributed masses on acoustic radiation behavior of plates,* Applied Acoustics, 69(3) (2008), pp. 272–279.

[25] C. HUANG AND S. NUTT, *Sound transmission prediction by 3-D elasticity theory,* Applied acoustics, 70(5) (2009), pp. 730–736.

[26] F. XIN, T. LU AND C. CHEN, *Dynamic response and acoustic radiation of double-leaf metallic panel partition under sound excitation,* Computational Materials Science, 46(3) (2009), pp. 728-732.

[27] X. ZHANG AND W. L. LI, *A unified approach for predicting sound radiation from baffled rectangular plates with arbitrary boundary conditions,* Journal of Sound and Vibration, 329(25) (2010), pp. 5307–5320.

[28] Z. HU, K. ZHOU AND Y. CHEN, *Sound radiation analysis of functionally graded porous plates with arbitrary boundary conditions and resting on elastic foundation,* International Journal of Structural Stability and Dynamics, 20(05) (2020), p. 2050068.

[29] U. ARASAN, F. MARCHETTI, F. CHEVILLOTTE, G. TANNER, D. CHRONOPOULOS AND E. GOURDON, *On the accuracy limits of plate theories for vibro-acoustic predictions,* Journal of Sound and Vibration, 493 (2021), p. 115848.

[30] K. ZHOU, L. ZHENKUN, X. HUANG AND H. HUA, *Vibration and sound radiation analysis of temperature-dependent porous functionally graded material plates with general boundary conditions,* Applied Acoustics, 154 (2019), pp. 236–250.

[31] N. CHANDRA, S. RAJA AND K. N. GOPAL, *Vibro-acoustic response and sound transmission loss analysis of functionally graded plates,* Journal of Sound and Vibration, 333(22) (2014), pp. 5786–5802.

[32] Q. GENG AND Y. LI, *Analysis of dynamic and acoustic radiation characters for a flat plate under thermal environments,* International Journal of Applied Mechanics, 4(03) (2012), p. 1250028.

[33] P. Oliazadeh, A. Farshidianfar and M. J. Crocker, *Study of sound transmission through single-and double-walled plates with absorbing material: Experimental and analytical investigation,* Applied Acoustics, 145 (2019), pp. 7–24.
[34] A. Le Bot, Foundation of Statistical Energy Analysis in Vibroacoustics, OUP Oxford, 2015.
[35] T. Yang, Q. Huang and S. Li, *Three-dimensional elasticity solutions for sound radiation of functionally graded materials plates considering state space method,* Shock and Vibration, (2016).
[36] D. Alpay, and I. Gohberg, The State Space Method: Generalizations and Applications, Springer Science & Business Media, vol. 161, 2006.
[37] J. Rayleigh, and R. B. Lindsay, The Theory of Sound, Two Volumes in One, 1945.
[38] J. U. Brackbill, and B. I. Cohen, Multiple Time Scales. Academic Press, 1985.
[39] A. Quarteroni, and G. Rozza, Reduced Order Methods for Modeling and Computational Reduction, Springer, vol. 9, 2014.
[40] J.-M. Dhainaut, X. Guo and C. Mei, *Nonlinear random response of panels in an elevated thermal-acoustic environment,* Journal of Aircraft, 40(4) (2003), pp. 683–691.
[41] H. Norouzi and D. Younesian, *Vibro-acoustic numerical analysis for the geometrically nonlinear viscoelastic rectangular plate subjected to subsonic compressible airflow,* Applied Acoustics, 174 (2021), p. 107779.
[42] A. Przekop and S. A. Rizzi, *Dynamic snap-through of thin-walled structures by a reduced-order method,* AIAA Journal, 45(10) (2007), pp. 2510–2519.
[43] G. Adomian, *A review of the decomposition method and some recent results for nonlinear equations,* Mathematical and Computer Modelling, 13(7) (1990), pp. 17–43.
[44] L. Gao, J. Wang, Z. Zhong, J. Du, *An analysis of surface acoustic wave propagation in functionally graded plates with homotopy analysis method,* Acta mechanica, 208(3-4) (2009), pp. 249–258.
[45] G. B. Folland, Introduction to Partial Differential Equations, Princeton University Press, vol. 102, 1995.
[46] X. Rui, G. Wang, and J. Zhang, Transfer Matrix Method for Multibody Systems: Theory and Applications. John Wiley & Sons, 2018.
[47] M. Golzari, and A. A. Jafari, *Sound transmission through truncated conical shells,* Applied Acoustics, 156 (2019), pp. 186–207.
[48] Y.-N. Kim, J.-S. Park, E.-S. Go, M.-H. Jeon and I.-G. Kim, *Nonlinear random response analyses of panels considering transverse shear deformations under combined thermal and acoustic loads,* Shock and Vibration, (2018).
[49] M. M. Zand and M. T. Ahmadian, *Application of homotopy analysis method in studying dynamic pull-in instability of microsystems,* Mechanics Research Communications, 36(7) (2009), pp. 851–858.
[50] F. Samadani, R. Ansari, K. Hosseini, and A. Zabihi, *Pull-in instability analysis of nanoelectromechanical rectangular plates including the intermolecular, hydrostatic, and thermal actuations using an analytical solution methodology,* Communications in Theoretical Physics, 71(3) (2019), pp. 349–356.
[51] T. Mori and K. Tanaka, *Average stress in matrix and average elastic energy of materials with misfitting inclusions,* Acta metallurgica, 21(5) (1973), pp. 571–574.
[52] N. Chandra, S. Raja and K. Gopal, A comprehensive analysis on the structural–acoustic aspects of various functionally graded plates, International Journal of Applied Mechanics, 7(05) (2015), p. 1550072.
[53] F. Alijani, F. Bakhtiari-Nejad and M. Amabili, *Nonlinear vibrations of FGM rectangular plates in thermal environments,* Nonlinear Dynamics, 66(3) (2011), pp. 251–270.

[54] J. N. REDDY, Mechanics of Laminated Composite Plates and Shells: Theory and Analysis, CRC Press, 2003.
[55] T. YANG AND Q. HUANG, *Vibro-acoustic response of FGM plates considering the thermal effects. in 2016 3rd International Conference on Materials Engineering,* Manufacturing Technology and Control. Atlantis Press, 2016.
[56] T. YANG AND Q. HUANG, *Sound radiation of functionally graded materials plates in thermal environment,* Composite Structures, 144 (2016), pp. 165–176.
[57] Y. LEE, X. ZHAO AND J. N. REDDY, *Postbuckling analysis of functionally graded plates subject to compressive and thermal loads,* Computer Methods in Applied Mechanics and Engineering, 199(25-28) (2010), pp. 1645–1653.
[58] R. N. MILES, Physical Approach to Engineering Acoustics, Springer, 2020.
[59] J. REDDY, AND C. CHIN, *Thermomechanical analysis of functionally graded cylinders and plates,* Journal of thermal Stresses, 21(6) (1998), pp. 593–626.
[60] M. AMABILI, Nonlinear Vibrations and Stability of Shells and Plates, Cambridge University Press, 2008.